Article

Cell Reports

Blocking Surgically Induced Lysyl Oxidase Activity Reduces the Risk of Lung Metastases

Graphical Abstract

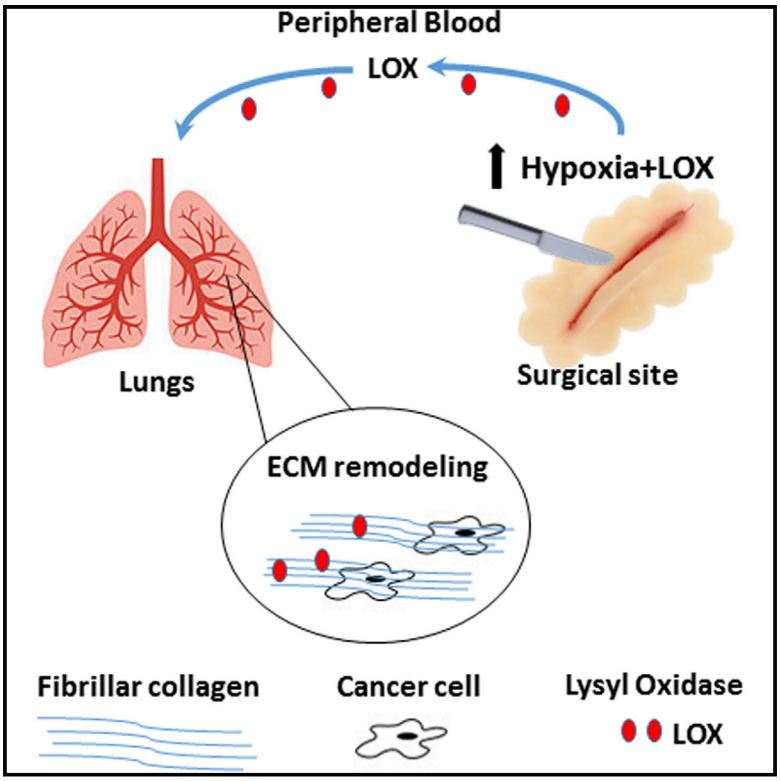

Highlights

- Surgery induces hypoxia and LOX expression at the wounded area
- Elevated LOX levels in plasma following surgery promote ECM remodeling in the lungs
- Tumor cell seeding is mediated by increased LOX activity in response to surgery
- Blocking LOX activity in peripheral blood hinders tumor cell seeding in the lungs

Authors

Chen Rachman-Tzemah, Shelly Zaffryar-Eilot, Moran Grossman, ..., Irit Sagi, Peleg Hasson, Yuval Shaked

Correspondence

phasson@technion.ac.il (P.H.), yshaked@technion.ac.il (Y.S.)

In Brief

Rachman-Tzemah et al. find that surgery promotes extracellular matrix (ECM) remodeling in the lungs due to increased lysyl oxidase activity. In turn, ECM remodeling contributes to tumor cell seeding and enhances metastasis. This study highlights effects that can occur in response to surgery and a potential impact on metastasis.

Rachman-Tzemah et al., 2017, Cell Reports *19*, 774–784
April 25, 2017
http://dx.doi.org/10.1016/j.celrep.2017.04.005

CellPress

OPEN ACCESS
CellPress

Cell Reports
Article

Blocking Surgically Induced Lysyl Oxidase Activity Reduces the Risk of Lung Metastases

Chen Rachman-Tzemah,[1] Shelly Zaffryar-Eilot,[2] Moran Grossman,[3] Dario Ribero,[4] Michael Timaner,[1] Joni M. Mäki,[5] Johanna Myllyharju,[5] Francesco Bertolini,[6] Dov Hershkovitz,[7] Irit Sagi,[3] Peleg Hasson,[2,*] and Yuval Shaked[1,8,*]

[1]Cell Biology and Cancer Science, Rappaport Faculty of Medicine, Technion, Haifa 31096, Israel
[2]Genetics and Developmental Biology, Rappaport Faculty of Medicine, Technion, Haifa 31096, Israel
[3]Biological Regulation, Weizmann institute of Science, Rehovot 7610001, Israel
[4]Department of Hepatobiliary and Pancreatic Surgery, European Institute of Oncology, Milan 20141, Italy
[5]Oulu Center for Cell-Matrix Research, Biocenter Oulu and Faculty of Biochemistry and Molecular Medicine, University of Oulu, Oulu 90220, Finland
[6]Laboratory of Hematology-Oncology, European Institute of Oncology, Milan 20141, Italy
[7]Department of Pathology, Tel Aviv Sourasky Medical Center, Tel Aviv 64239, Israel
[8]Lead Contact
*Correspondence: phasson@technion.ac.il (P.H.), yshaked@technion.ac.il (Y.S.)
http://dx.doi.org/10.1016/j.celrep.2017.04.005

SUMMARY

Surgery remains the most successful curative treatment for cancer. However, some patients with early-stage disease who undergo surgery eventually succumb to distant metastasis. Here, we show that in response to surgery, the lungs become more vulnerable to metastasis due to extracellular matrix remodeling. Mice that undergo surgery or that are preconditioned with plasma from donor mice that underwent surgery succumb to lung metastases earlier than controls. Increased lysyl oxidase (LOX) activity and expression, fibrillary collagen crosslinking, and focal adhesion signaling contribute to this effect, with the hypoxic surgical site serving as the source of LOX. Furthermore, the lungs of recipient mice injected with plasma from post-surgical colorectal cancer patients are more prone to metastatic seeding than mice injected with baseline plasma. Downregulation of LOX activity or levels reduces lung metastasis after surgery and increases survival, highlighting the potential of LOX inhibition in reducing the risk of metastasis following surgery.

INTRODUCTION

Surgical resection of tumors is a common therapeutic procedure, especially for early-stage localized, and potentially curative, disease. While surgery can ultimately cure many patients, such as those with early-stage disease, distant macroscopic metastasis can emerge in others months to years later (Demicheli et al., 2008; van der Bij et al., 2009). It has been reported that 25%–30% of colorectal cancer patients who have no visible metastasis at the time of diagnosis will develop distant metastases within 5 years after primary tumor resection, which in some cases may be related to the effects of the surgery (van der Bij et al., 2009). Similarly, high risk of recurrence for early-stage breast cancer patients following mastectomy has been reported in an analysis of 1,173 patients who underwent mastectomy with no subsequent adjuvant systemic therapy (Demicheli et al., 1996). Mechanisms to explain distant metastasis following primary tumor resection include (1) the presence of residual tumor cells or tissue at the resected site (Ando et al., 2003; Minsky et al., 1988), (2) the recruitment of inflammatory cells and platelets to the resected site that promote wound healing and cell proliferation (Ceelen et al., 2014; Hofer et al., 1999; Retsky et al., 2012), and (3) increased local and systemic effects that can induce an angiogenic switch in remote dormant tumors (Bono et al., 2010; Retsky et al., 2012; Takemoto et al., 2012).

The seeding of tumor cells at metastatic organ sites is a multistep process. Previous studies have revealed that hypoxic tumor cells stimulate angiogenic-related factors via HIF1-α, leading to increased tumor invasion (Paraskeva et al., 2006; Semenza, 2012). HIF1-α expression in tumors can also upregulate lysyl oxidase (LOX) (Erler et al., 2006), a member of the secreted copper-dependent amine oxidases known to covalently crosslink collagens and elastin in the extracellular matrix (ECM) (Barker et al., 2012). LOX is expressed by different cell types, including tumor cells and stromal cells within the tumor microenvironment (Decitre et al., 1998). It has been shown that increased LOX expression in tumors accounts for the recruitment of $CD11b^+$ bone-marrow-derived cells (BMDCs) at distant organs, contributing to the formation of a niche and facilitating a pre-metastatic microenvironment for tumor cell seeding (Erler et al., 2009). Thus, LOX plays an important role in tumor growth and metastasis. However, the contribution of LOX to tumor cell seeding and subsequently to metastasis soon after surgery is unknown.

The host response to anti-cancer therapy and its contribution to tumor (re)growth and metastasis has been evaluated following chemotherapy (Daenen et al., 2011; Gingis-Velitski et al., 2011), radiotherapy (Barcellos-Hoff et al., 2005; Timaner et al., 2015), and various molecularly targeted drugs (Beyar-Katz et al., 2016) (for a review, see Shaked, 2016). Here, we evaluated remote (pulmonary) changes in LOX expression and activity in

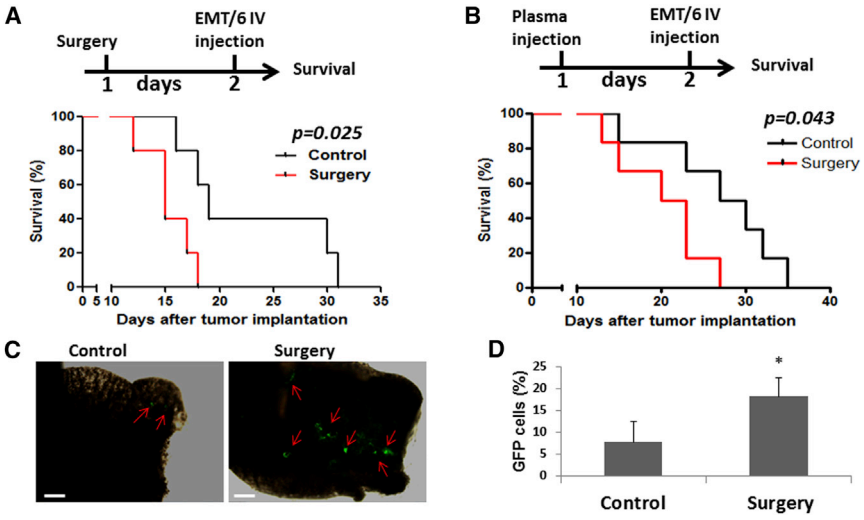

Figure 1. Increased Mortality Rate in Post-surgery Mice

(A) A 1 cm incision in the abdomen of non-tumor-bearing 8- to 10-week-old BALB/c mice was performed. Control mice did not undergo any surgical procedure (n = 5 mice /group). After 24 hr, the mice were injected with 2.5 × 10^4 EMT/6-GFP+ cells through the tail vein to obtain an experimental lung metastasis model. Mouse survival was monitored daily, and a Kaplan-Meier survival curve was plotted (p = 0.025).

(B) Plasma drawn from control or post-surgery mice was intraperitoneally injected into naive 8-10-week-old BALB/c mice (100 μL/mouse; n = 6 mice/group). After 24 hr, 2.5 × 10^4 EMT/6-GFP+ cells were injected through the tail vein to obtain experimental lung metastases, and survival was monitored. Kaplan-Meier survival curve is shown (p = 0.043).

(C and D) Mice (n = 3 mice/group) were injected with plasma as in (B). After 24 hr, mice were injected with the EMT/6-GFP+ (2.5 × 10^4) cells, and 15 min later, PuMA was performed. Subsequently, lungs were removed and sectioned. Lung slices were cultured in medium for 6 days, and GFP+ cells were detected by fluorescence microscopy. Red arrows indicate GFP+ cells. Scale bar, 200 μm (C). Subsequently, lung sections were prepared as single-cell suspensions. The percentage of GFP+ cells was quantified by flow cytometry (D). LOX activity was assessed by paired Student's t test for three biological replicates. The survival experiments were repeated twice, and representative Kaplan-Meier curves are provided. *p < 0.05, as assessed by Student's t test.

All error bars represent SD.

response to surgery and their contribution to tumor cell seeding and metastasis.

RESULTS

Host Response to Surgery Promotes Metastasis

Increased metastases after localized tumor resection in some cases could be due to systemic changes that affect various host tissues in response to surgery. Previous clinical studies indicated that both systemic and local angiogenesis are induced in response to surgery when compared to laparoscopy (Bono et al., 2010). To test whether our surgical mouse model induces angiogenesis, we performed a surgical procedure in non-tumor-bearing mice involving a 1 cm incision in the peritoneum followed by suturing. Thereafter, we evaluated the levels of circulating bone-marrow-derived proangiogenic cells over time and the extent of local angiogenesis following surgery. A significant increase in the number of viable circulating endothelial cells (CECs) and endothelial progenitor cells (CEPs) was observed at several time points following surgery (Figure S1A). Likewise, increases in microvessel density in Matrigel plugs, in vitro human umbilical vein endothelial cell (HUVEC) microvessel tube formation, and microvessel sprouting from murine aortic rings were observed in the presence of plasma obtained from post-surgery mice compared to control (Figure S1B–S1D). Thus, the surgical procedure in our mouse model mimics host angiogenic effects reported in certain clinical circumstances.

We next evaluated the host-derived effects of surgery on tumor cell seeding and growth in metastatic sites. We employed an experimental lung metastasis assay using the murine EMT/6-GFP+ breast cancer cell line. Control mice and mice that previously underwent surgery were intravenously injected with tumor cells, which subsequently seeded in the lungs. Survival was then monitored over time. Mortality rates were increased in post-surgery mice compared to controls (Figure 1A). Similarly, recipient mice injected with 100 μl plasma from donor mice that had undergone surgery exhibited an increased mortality rate in comparison to mice injected with control plasma (Figure 1B), indicating that a host effect, expressed within the plasma, in response to surgery rather than the actual surgical procedure is responsible for the observed effects. To directly assess tumor cell seeding in the lungs, regardless of any host responses that may affect tumor cells per se while seeding and proliferating at the metastatic sites, a pulmonary metastatic assay (PuMA) was performed using the EMT/6-GFP+ cell line. In this assay, the potential of tumor cell seeding is solely dependent on tumor cells binding to the lungs and not systemic effects that could affect tumor cell proliferation. The number of GFP+ tumor cells present in the lungs of mice that underwent surgery was substantially elevated in comparison to control mice (Figures 1C and 1D). Taken together, our results suggest that enhanced tumor cell seeding is a result of remote changes occurring, in part, in the pre-metastatic (lung) tissue in response to surgery.

Increased Mortality Rate in Mice that Undergo Surgery Is Mediated by LOX Activity in the Lungs

ECM remodeling is one of the main factors that can facilitate tumor cell seeding; LOX mediates collagen crosslinking and therefore is a key regulator of ECM remodeling (Barker et al., 2012). Recent studies have shown that LOX is expressed by tumor cells, and serves as a key enzyme promoting metastasis by contributing to a pre-metastatic niche (Cox et al., 2015; Erler et al., 2006, 2009). In our model, we found that LOX expression and activity were significantly upregulated at the hypoxic

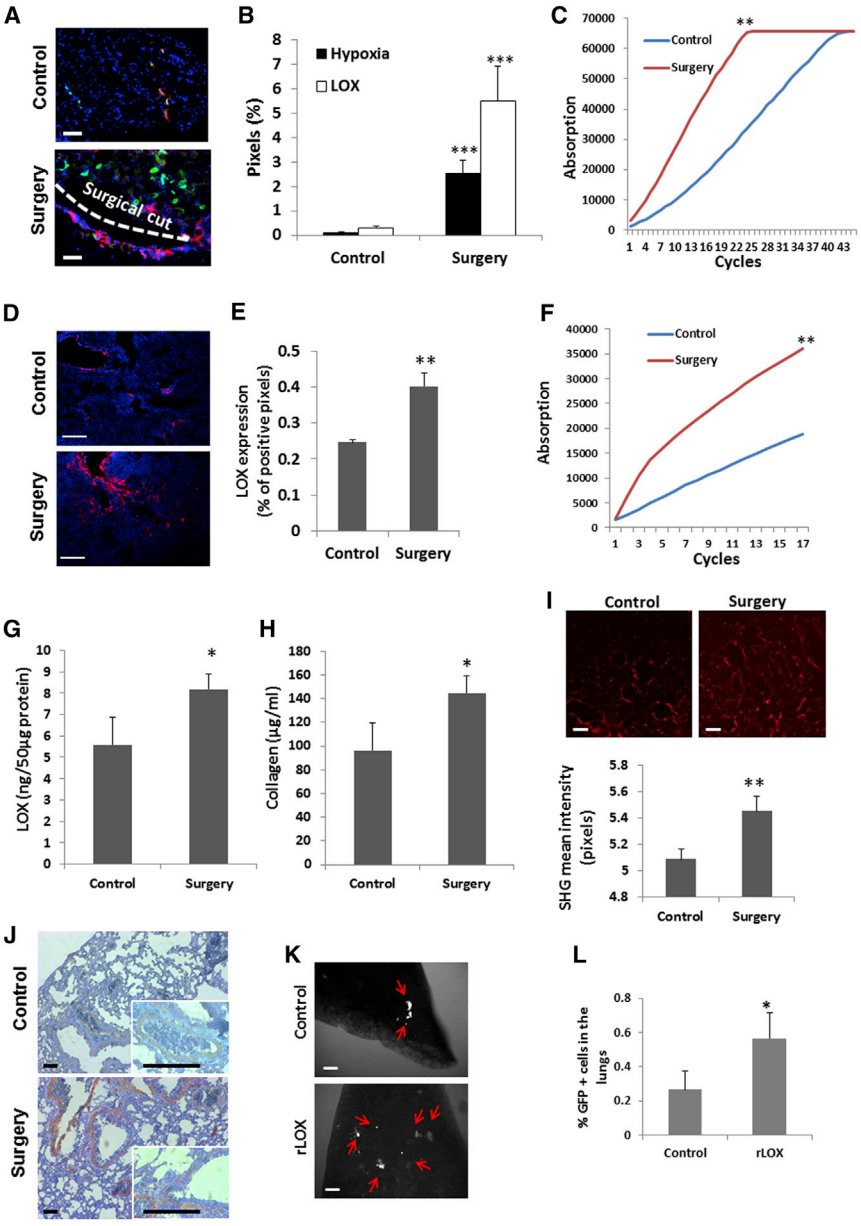

Figure 2. High Expression of LOX following Surgery Correlates with Increased Pulmonary Metastasis

(A–C) A 1 cm incision in the abdomen of non-tumor-bearing 8- to 10-week-old BALB/c mice was performed. Control mice did not undergo any surgical procedure (n = 5 mice /group). After 24 hr, mice were injected with pimonidazole, and 90 min later, the peritoneum was excised, embedded in OCT, and cryosectioned. (A) Sections were immunostained for LOX (green) and hypoxia (red). Nuclei were stained with DAPI (blue). Dashed line marks the incision site. Scale bar, 200 μm. (B) Quantification of the percentage of LOX- and hypoxia-positive pixels is presented (n > 15 field/group). (C) Peritoneum lysates (n = 3 mice/group) were evaluated for LOX activity.

(D–H) Lungs from 8- to 10-week-old BALB/c control mice or 24 hr after mice underwent surgery (n = 3 mice/group) were sectioned and immunostained for LOX (red). Nuclei were stained with DAPI (blue). Scale bar, 200 μm (D). Quantification of LOX expression in lung sections by means of percentage of positive pixels is presented (E). Lung lysates (n = 3 mice/group) were evaluated for LOX activity (F) and expression (G). LOX activity was assessed by paired Student's t test for three biological replicates. (H) Lungs from 8- to 10-week-old BALB/c control mice or 72 hr after surgery (n = 3 mice/group) were assessed for new collagen formation.

(I) Two-photon second harmonic generation (SHG) imaging depicting fibrillary collagens (red) in the lungs of control and post-surgery mice. Scale bar, 50 μm. Relative collagen intensity was determined using densitometric analysis (ImageJ).

(J) In a parallel experiment to (D)–(H), lungs were removed and embedded in paraffin. Lung sections were immunostained for LOX (brown). Counterstaining was performed using hematoxylin. Images were captured at 100× (large micrograph) and 400× (small micrograph) magnifications. Scale bar, 100μm.

(K and L) 8- to 10-week-old BALB/c mice (n = 3 mice/group) were injected with recombinant LOX (rLOX, 25 μg/kg) or PBS. After 24 hr, the mice were intravenously injected with EMT/6-GFP+ cells (2.5×10^4 cells/mouse) and processed for PuMA. Lung slices were cultured in medium for 6 days, and GFP+ cells were detected by fluorescence microscopy (Olympus SZX9 fluorescence stereo microscope). Red arrows indicate GFP+ cells. Scale bar, 200 μm (K). Subsequently, all lung slices were prepared as single-cell suspensions, and the percentage of GFP+ cells was quantified using flow cytometry (L). *$p < 0.05$ and **$p < 0.01$ using Student's t test.
All error bars represent SD.

surgical site in the wounded peritoneum in comparison to control peritoneum (Figures 2A–2C). Specifically, high-magnification images of the surgical site revealed intracellular LOX expression of peritoneal myofibers (Figure S2A). Furthermore, LOX expression and activity, quantity of newly synthesized collagen, and fibrillar collagen expression were all significantly higher in the lungs of mice that underwent surgery than in the lungs of control mice (Figures 2D–2I). Notably, high LOX extracellular staining was located mainly in the lung stroma surrounding the bronchioles in post-surgery lungs when compared to control lungs (Figure 2J). However, high-magnification images detected intracellular LOX expression in different cell types, with no noticeable differences in expression pattern between control and post-surgery lungs, suggesting that the major source of LOX in the lungs of post-surgery mice is from the remote surgical site (Figure S2B). In addition, a significant decrease in LOX expression and activity was found in the liver of mice that underwent surgery compared to control mice, whereas no significant changes were observed in the spleen (Figures S2C and S2D). Importantly, 24 hr after surgery, the percentage of $CD11b^+$ cells in the pre-metastatic lungs

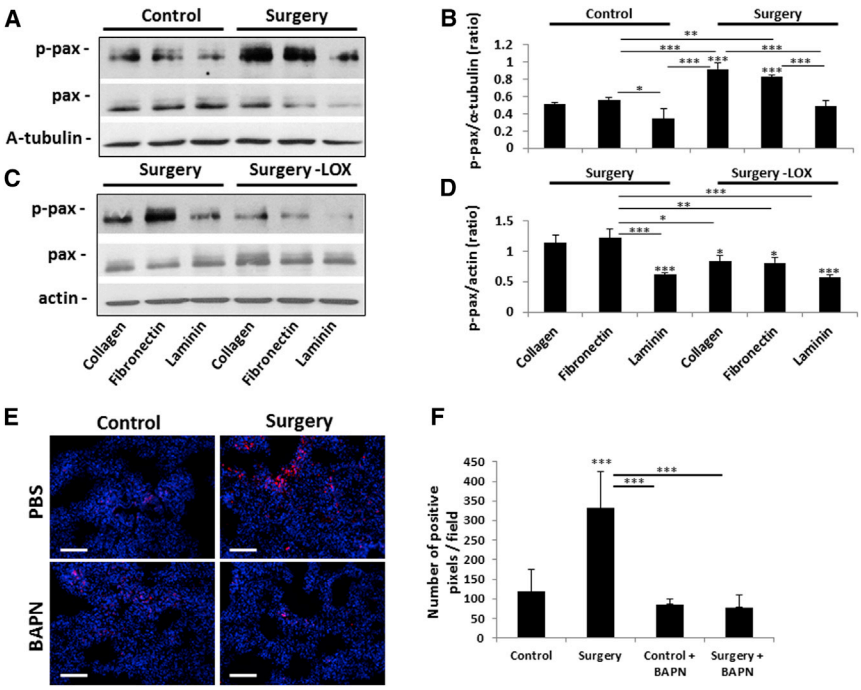

Figure 3. Plasma from Mice that Undergo Surgery Induces Focal Adhesion Signaling in Tumor Cells

(A–D) MCF7 cells were cultured in the presence of collagen, fibronectin, or laminin that were primed with (A) plasma from control or post-surgery mice or (C) plasma from post-surgery mice that was either untreated or depleted of LOX (Surgery-LOX). The levels of total paxillin (pax) and p-pax in cell lysates were evaluated by western blotting. α-Tubulin (A) or actin (C) served as loading controls. The ratios between p-pax and α-tubulin or actin (loading controls) were calculated by densitometry analysis (B and D, respectively). The western blot represents three biological repeats.

(E and F) Lungs from 8- to 10-week-old BALB/c control or post-surgery mice (n = 3 mice/group) that were treated with PBS or BAPN for three sequential days were sectioned and immunostained for p-pax (red). Nuclei were stained with DAPI (blue). Scale bar, 200 μm (E). Quantification of p-pax expression in lung sections by means of positive pixels is shown in (F). *$p < 0.05$, **$p < 0.01$, and ***$p < 0.001$ using one-way ANOVA followed by Tukey post hoc test.

All error bars represent SD.

of post-surgery mice was comparable to that in control mice (Figures S2E and S2F), ruling out the possibility of the formation of a reported pre-metastatic niche at this early time point (Erler et al., 2009; Kaplan et al., 2005; Psaila et al., 2006). These results indicate that the immediate effects of surgery are primarily associated with ECM remodeling. In order to strengthen the hypothesis that LOX is a major contributor to metastatic seeding in the lungs within hours of surgery, a PuMA, which measures cell seeding in the lungs, was carried out on mice 24 hr after they were injected with recombinant LOX, the function of which was evaluated by a LOX activity assay (Figure S2G). An increased number of metastatic cells was found in the lungs of mice injected with recombinant LOX compared to control mice injected with PBS (Figures 2K and 2L).

The seeding of cells in collagen and ECM is regulated in part by integrin signaling pathways (Larsen et al., 2006). One of the major readouts of integrin signaling is paxillin, a scaffold protein connecting focal adhesion kinase to the actin cytoskeleton (Turner et al., 1990; Zaidel-Bar et al., 2007). We therefore sought to determine the level of phospho-paxillin (p-pax) in MCF-7 breast carcinoma cells, a cell line with minimal LOX expression (Kraft-Sheleg et al., 2016), in response to plasma from control or post-surgery mice. MCF-7 cells were seeded on collagen, laminin, or fibronectin, all of which are ligands of integrins (Heino and Käpylä, 2009), in the presence or absence of plasma from control or post-surgery mice. Increased expression of p-pax was observed with all three ligands in the presence of plasma from post-surgery mice compared to control, with laminin producing the weakest effect (Figures 3A and 3B). In addition, when the same experiment was performed using plasma from post-surgery mice depleted of LOX, the expression of p-pax was found to be lower than the post-surgery non-depleted plasma group (Figures 3C and 3D), suggesting that LOX expression mediates focal adhesion signaling. Furthermore, expression of p-pax was higher in the lungs of mice that underwent surgery than in control mice, an effect that could be inhibited by treating the mice with β-aminoproprionitrile (BAPN), an irreversible competitive inhibitor of all LOX family members (Bondareva et al., 2009) (Figures 3E and 3F). It should be noted that all three ligands are substrates of LOX as assessed by the oxidation assay, whereas laminin was the least effective substrate, in line with the results shown in Figures 3A–3D (Figure S3A). Taken together, increased LOX activity in the lungs soon after the mice undergo surgery contributes to tumor cell seeding via focal adhesion signaling, suggesting interactions between integrins and LOX ligands in the remodeled ECM.

LOX Inhibition following Surgery Reduces Metastasis and Increases Survival

As LOX contributes to the seeding of tumor cells in the lungs, we next studied the effects of LOX inhibition in mice using BAPN. Plasma from control mice or mice that underwent surgery was injected into recipient naive mice. After 24 hr, the recipient mice were injected with EMT/6-GFP+ cells to obtain the experimental lung colonization metastasis assay described above. BAPN monotherapy did not affect the percentage of GFP+ cells in the lungs of control mice. In contrast, the increase in percentage of GFP+ cells in the lungs of mice injected with plasma obtained from the post-surgery mice was completely abolished by the BAPN therapy (Figures 4A and 4B), and their mortality rate was reduced, as assessed in a parallel experiment (Figure 4C). No significant changes in mortality rate and percentage of

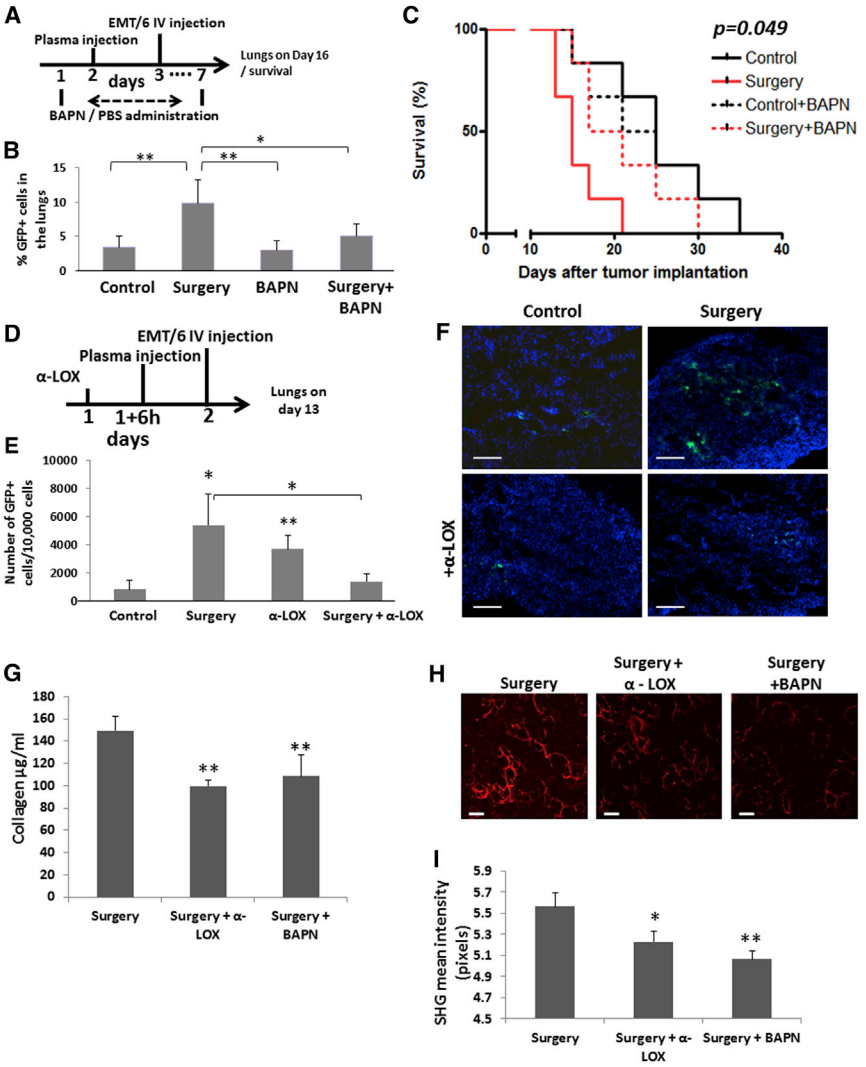

Figure 4. Blocking LOX Activity in Mice that Undergo Surgery Decreases Tumor Cell Seeding in the Lungs and Increases Survival

(A–C) 8- to 10-week-old BALB/c mice were treated with PBS or BAPN (LOX inhibitor, 100 mg/kg) daily for seven consecutive days. On day 2, the mice were injected with 100 µL plasma from control or post-surgery mice. On day 3, EMT/6-GFP+ cells (2.5×10^4) were injected through the tail vein to obtain an experimental lung metastasis assay. A scheme of the experimental procedure is shown in (A). On day 13 after tumor cell injection, lungs were removed and prepared as single-cell suspensions (n = 4 mice/group). The percentage of GFP+ cells was quantified by flow cytometry (B). In a parallel experiment, survival of control and BAPN-treated mice injected with plasma from mice that underwent surgery or control mice was monitored. A Kaplan-Meier survival curve is shown (n = 6 mice/group, p = 0.049) (C).

(D–F) 8- to 10-week-old BALB/c mice were treated with PBS control or 20 mg/kg anti-LOX antibodies (n = 4 mice/group). After 6 hr, the mice were intraperitoneally injected with plasma from control or post-surgery mice (100 µL/mouse). On day 2, mice were injected through the tail vein with 2.5×10^4 EMT/6-GFP+ cells to obtain an experimental lung metastasis model. (D) A scheme of the experimental procedure is shown. (E) On day 13 after tumor cell injection, lungs were removed and prepared as single-cell suspensions. The number of GFP+ cells in the lungs was evaluated by flow cytometry. (F) In a parallel experiment, lung sections (n = 5 mice/group) were counterstained with DAPI and analyzed by fluorescence microscopy for the presence of GFP+ cells. Scale bar, 200µm.

(G–I) Lungs from 8- to 10-week-old BALB/c mice 72 hr after surgery (n = 3 mice/group) that were treated with anti-LOX antibodies (α-LOX; 20 mg/kg) or BAPN (100 mg/kg) were assessed for new collagen formation (G). (H) Two-photon second harmonic generation (SHG) imaging depicting fibrillary collagens (red) in the lungs of post-surgery mice treated with anti-LOX or BAPN. Scale bar, 50 µm. (I) Relative collagen intensity was determined using densitometric analysis (ImageJ). *p < 0.05 and **p < 0.01 using one-way ANOVA followed by Tukey post hoc test.

All error bars represent SD.

GFP+ cells in the lungs of control mice treated with BAPN or PBS control were found (Figures 4B and 4C). Importantly, escalating doses of BAPN in a range of 0–10 mg/mL did not contribute to tumor cell apoptosis (Figure S3B), suggesting that the therapeutic effect of BAPN is related to the inhibition of LOX activity. Furthermore, inhibiting LOX using specific anti-LOX activity-inhibiting antibodies similarly reduced tumor cell seeding in the lungs of mice injected with plasma from post-surgery mice, indicating that the effect is largely regulated by LOX. Of note, it is not clear why blocking LOX in control mice increased metastatic cell seeding (Figures 4D–4F). It is possible that other bypass pathways may play a role similar to MMP9 inhibition in control mice as previously described (Gingis-Velitski et al., 2011; Shchors et al., 2013). Moreover, fibrillar collagen and newly synthesized collagen quantities in the lungs of mice 3 days after localized peritoneal surgery were significantly increased when compared to lungs obtained from post-surgery mice treated with BAPN or anti-LOX antibodies (Figures 4G–4I). Of note, both anti-LOX and BAPN reduced LOX activity in the lungs, while control rabbit immunoglobulin G (IgG) had no effect (Figures S3C and S4, respectively). To further strengthen our results, we wished to rule out the possibility that inflammation-induced pulmonary vessel permeability mediates the increased tumor cell seeding in the lungs at this early time point. Evans blue assay performed on mice 24 hr after they underwent surgery revealed that pulmonary vessel permeability was not significantly different in post-surgery mice compared to control mice (Figure S5A), suggesting that tumor cell seeding was not affected by inflammation. Additionally, the number and percentage of tumor cells (EMT/6-GFP+) seeded in the lungs 20 min after tail vein injection of 2×10^5 cells (10-fold higher than the number of cells injected in the PuMA) were significantly higher in post-surgery mice than in

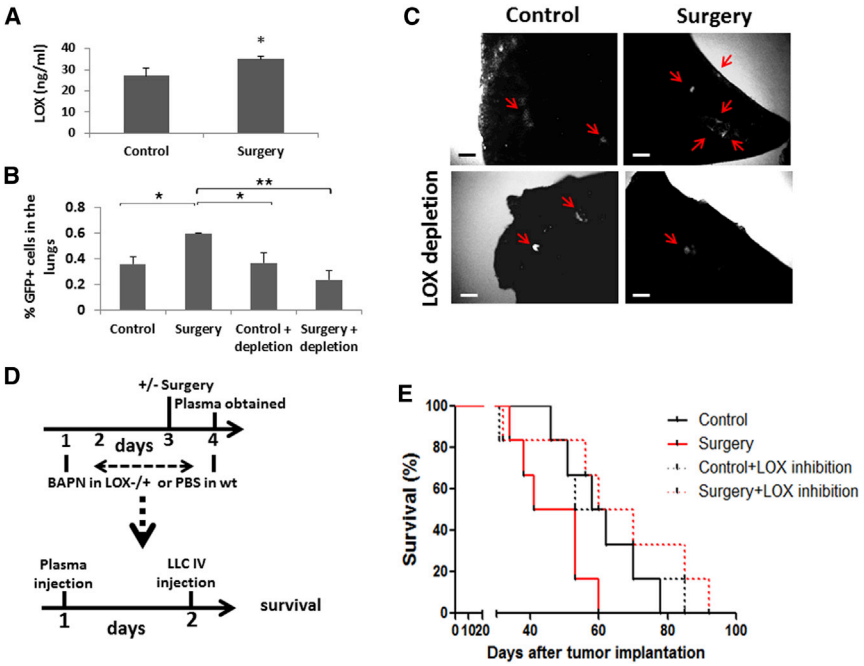

Figure 5. LOX-Depleted Plasma of Post-surgery Mice Inhibits Tumor Cell Seeding in the Lungs and Increases Survival

(A) Plasma obtained from control non-tumor-bearing BALB/c mice, or 24 hr after the mice underwent abdominal surgery was evaluated for LOX expression (n = 4 mice/group). *p < 0.05 as assessed by Student's t test. (B and C) LOX was depleted from plasma drawn from control and post-surgery mice as described in Experimental Procedures. The plasma was injected into 8- to 10-week-old naive BALB/c mice (n = 3 mice/group), and 24 hr later, EMT/6-GFP+ cells (2.5×10^4) were intravenously injected and processed for PuMA. Lung sections were cultured for 6 days.

(B) The percentage of GFP+ cells was quantified by flow cytometry after lung tissues were prepared as single-cell suspensions.

(C) Fluorescent images of lung slices were captured by fluorescence microscopy system. Scale bar, 200μm. *p < 0.05; **p < 0.01 using one-way ANOVA followed by Tukey post hoc test.

(D and E) C57BL/6-LOX$^{+/-}$ mice and their wild-type counterparts were injected with BAPN (100 mg/kg) and PBS, respectively, for four consecutive days. On day 3, half of the mice from each group underwent abdominal surgery. After 24 hr, plasma from each group of mice was drawn and pooled. The plasma was then injected to naive 8- to 10-week-old C57BL/6 mice, and 24 hr later, LLC-GFP+ cells (2.5×10^4) were intravenously injected through the tail vein to generate lung metastases (n = 6 mice/group). (D) A scheme of the experimental procedure is shown. (E) A Kaplan-Meier survival curve is shown. Statistical significance was achieved only when comparing surgery and surgery + LOX inhibition groups (p = 0.043).

All error bars represent SD.

control mice. This effect was dramatically reduced when the mice were also treated with BAPN as assessed by microscopic imaging of lung specimens and flow cytometry of single-cell suspensions from dissociated lungs (Figures S5B and S5C). Taken together, LOX-induced ECM remodeling accounts for tumor cell seeding in the lungs of post-surgery mice.

The fact that plasma derived from post-surgery mice had the same effect on tumor cell seeding as surgery itself suggested it entails the factor mediating this activity. Therefore, LOX levels were evaluated in the plasma of control and post-surgery mice. The plasma of post-surgery mice exhibited significantly elevated LOX levels compared to plasma from control mice, suggesting that LOX upregulation in the plasma may affect tumor cell seeding in the lungs (Figure 5A). To test this possibility, we depleted LOX from plasma of control mice and mice that underwent surgery and assessed tumor cell seeding using PuMA in recipient mice injected with the different plasma samples. Whereas LOX depletion did not affect tumor cell seeding in the control group, it significantly decreased tumor cell seeding in the surgery group (Figures 5B and 5C). In a parallel experiment, plasma was obtained from untreated wild-type mice or BAPN-treated LOX heterozygous mice (Mäki et al., 2002) that either underwent surgery or not. The plasma was then injected into mice, and survival was assessed in an experimental lung metastasis assay. LOX inhibition did not affect survival of the control group. However, in the surgery group, survival times were increased when LOX was inhibited (Figures 5D and 5E; statistical significance [p = 0.043] was reached when comparing surgery with surgery + LOX depletion groups). Collectively, our results suggest that LOX in the plasma from post-surgery mice promotes tumor cell seeding, and its depletion inhibits collagen synthesis and ECM remodeling.

LOX Contributes to Metastasis following Surgery in Clinically Relevant Models

To bolster the possibility that our results may be clinically relevant, we employed two different experimental approaches. In the first, we used a more clinically relevant tumor mouse model of metastasis, in which spontaneous metastases appear in the lungs after resection of a primary orthotopic 4T1 murine breast cancer. To inhibit LOX, BAPN was administered for 7 consecutive days after tumors were resected. BAPN-treated mice exhibited significantly extended survival and reduced lung metastasis in comparison to mice that did not receive treatment after surgery (Figures 6A–6D). In the second approach, plasma was drawn from colorectal cancer patients at baseline and 24 hr after they underwent abdominal surgery (n = 6). The plasma was injected into mice, and metastases were evaluated using EMT/6-GFP+ cells in an experimental lung metastasis assay. In five out of six cases, the post-surgery plasma induced higher numbers of lung metastases in comparison to baseline plasma (Figures 6E and 6F). Such post-surgical plasma also induced ECM remodeling and increased fibrillar collagen expression as well as LOX activity in the lungs in a manner similar to that found in mice that underwent abdominal surgery (Figures 6G, S6A, and S6B). Importantly, pooled plasma obtained from patients that underwent surgery that was depleted of LOX did not increase

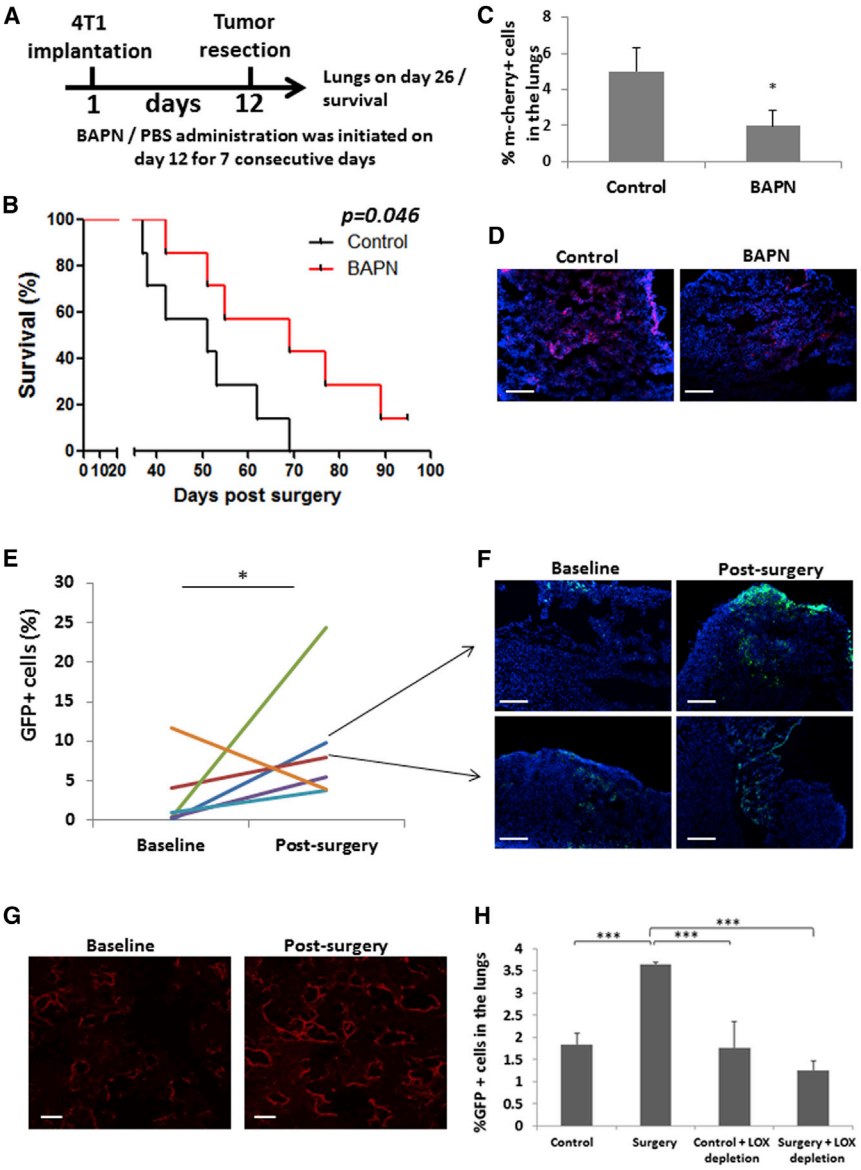

Figure 6. LOX Inhibition in Clinically Relevant Tumor Models Increases Survival and Reduces Tumor Cell Seeding in the Lungs

(A–D) 8- to 10-week-old BALB/c mice were used as recipients for orthotopic transplantation of 4T1-mCherry+ cells into the mammary fat pad. When primary tumors reached 150–200 mm^3 (day 12), they were resected, and treatment with BAPN (100 mg/kg) or PBS was initiated. The treatment was administered for seven consecutive days. A scheme of the experimental procedure is shown (A). Mouse survival was monitored, and a Kaplan-Meier survival curve was plotted (n = 7 mice/group) (B). In a parallel experiment, 26 days after primary tumor resection, lungs were removed and either prepared as single-cell suspensions or sectioned. The percentage of mCherry+ cells in the lung suspensions was quantified by flow cytometry (n = 5 mice/group) (C). Lung sections were counterstained with DAPI and analyzed by fluorescence microscopy (n = 5 mice/group). Representative images are shown (mCherry+ cells, red; nuclei, blue). Scale bar, 200 μm (D). *$p < 0.05$, as assessed by Student's t test.

(E and F) Plasma samples obtained from colorectal cancer patients at baseline or 24 hr after abdominal surgery (n = 6 patients) were intraperitoneally injected into 8- to 10-week-old CB.17 SCID mice (n = 3 mice/plasma specimen). After 24 hr, mice were intravenously injected with 2.5 × 10^4 EMT/6-GFP+ cells. After 12 days, lungs were removed and either prepared as single-cell suspensions or sectioned. The percentage of GFP+ cells in the lung suspensions was quantified by flow cytometry (E). Lung sections were stained with DAPI and analyzed by fluorescence microscopy. Representative images of lung sections from mice injected with the indicated patient plasma are shown (GFP+ cells, green; nuclei, blue). Scale bar, 200 μm (F). (G) Two-photon second harmonic generation mode (SHG) imaging depicting fibrillary collagens (red) in the lungs of mice injected with control plasma and plasma from patients 24 hr after surgery. Scale bar, 50 μm. Relative collagen intensity was determined using densitometric analysis (ImageJ) as presented in Figure S6A. (H) Plasma (pooled) from colorectal cancer patients (n = 6) at baseline or 24 hr after surgery was depleted of LOX as described in Experimental Procedures. Subsequently, the plasma was injected peritoneally into naive SCID CB.17 mice (n = 3 mice/group), and 24 hr later, EMT/6-GFP+ cells (2.5 × 10^4) were intravenously injected for PuMA. Lungs were cultured for 6 days and then visualized by fluorescence microscopy as shown in Figure S6C. Subsequently, lung sections were prepared as single-cell suspensions, and the percentage of GFP+ cells in the lungs was quantified by flow cytometry. ***$p < 0.01$ using one way ANOVA followed by Tukey post hoc test.

All error bars represent SD.

metastatic seeding in the lungs as assessed by PuMA (Figures 6H and S6C).

DISCUSSION

The notion that tumor cells remaining at the site of a surgical resection can re-grow and sometimes even spread may contribute to inferior outcomes in both clinical and preclinical scenarios (Coffey et al., 2003; DeLisser et al., 2009; James et al., 2011). Here, we describe an additional explanation for possible spread of metastasis following surgery. We find that the host, in response to surgery, conditions potential metastatic sites to facilitate tumor cell seeding. We demonstrate that mice that undergo abdominal surgery and are subsequently injected with tumor cells via the tail vein succumb to extensive metastatic lesions earlier than controls. These mice exhibit structural changes in the ECM at the site of metastasis due to an increase in newly synthesized collagen. We show that these effects are mediated by LOX. LOX activity and expression are substantially enhanced in the lungs of mice following surgery, as well as in

mice pre-conditioned with plasma from donor mice that underwent surgery. Accordingly, we find that the surgery is associated with release of LOX to the circulation from the hypoxic wounded site, which in turn induces the formation of the pre-metastatic sites. Such pro-metastatic effects are abolished following LOX inhibition (e.g., using BAPN, neutralizing antibodies for LOX, or LOX depletion from plasma). Notably, antibodies only neutralize extracellular LOX and therefore act primarily on the ECM rather than on LOX intracellular targets.

LOX has been implicated as a key enzyme contributing to the pre-metastatic niche promoting the recruitment of $CD11b^+$ cells to future metastatic sites measured within weeks after primary tumor cell implantation (Erler et al., 2009). Furthermore, increased activity of LOX and collagen crosslinking have been shown to promote fibrosis and subsequent metastasis (Cox et al., 2013). In our study, we focused on the immediate contribution of LOX to metastasis by means of ECM remodeling, which promotes the seeding of tumor cells in the lungs within hours following surgery. At this time point, no changes in $CD11b^+$ cells colonizing the pre-metastatic sites were observed, and there was no significant difference in pulmonary permeability, suggesting that inflammation at this early time point did not contribute to tumor cell seeding. However, it should be noted that clinically, the use of ketorolac (an analgesic drug with non-steroidal anti-inflammatory properties) in surgery resulted in superior disease-free survival of breast cancer patients who underwent mastectomy compared to patients who underwent mastectomy but were not treated with ketorolac (Retsky et al., 2012).

Erler et al. have demonstrated that LOX is a key regulator of metastasis that is induced by hypoxia. LOX expression in hypoxic tumors correlates with increased incidence of metastasis in patients with breast and head and neck cancers. Accordingly, the blockade of LOX in mice bearing orthotopic breast cancers results in decreased tumor cell invasiveness and metastasis (Erler et al., 2006). In addition, bone metastasis of triple negative breast cancer cells is associated with hypoxia and LOX activity (Cox et al., 2015). LOX family members promote endothelial cell activity and angiogenesis in tumors and support ECM remodeling (Baker et al., 2013; Zaffryar-Eilot et al., 2013). Therefore, antiangiogenic therapy, which induces hypoxia in tumors (Blagosklonny, 2001), may lead to increased LOX expression. As a result, alterations in ECM may take place in distant sites (e.g., lungs or liver) that can decrease the therapeutic response to therapy. These effects may also explain why, at least pre-clinically, antiangiogenic drugs sometimes promote metastasis (Ebos et al., 2009; Pàez-Ribes et al., 2009; Rahbari et al., 2016). Testing ECM structure in different organs in response to antiangiogenic therapy is therefore worthy.

The question remains why LOX has a significant effect on ECM remodeling in the lungs while its expression and activity in other organs are reduced or do not change in post-surgery mice when compared to control mice. It is possible that the high oxygen concentration in lung tissue contributes to LOX enzymatic activity. Abundant microvessel networks in the lungs contribute to increased oxygen availability, which in turn promotes LOX enzymatic activity (Barker et al., 2012). This may explain the increased LOX enzymatic activity in the lungs compared to other organs. Thus, the level of ECM remodeling could be higher in lung stroma than in other tissues.

Our results may also have clinical implications. Mice bearing tumors that spontaneously metastasize exhibit a reduced mortality rate when LOX is inhibited following surgery. Additionally, mice preconditioned with plasma from post-surgery colorectal cancer patients exhibit an increased number of metastatic cells in the lungs compared to mice injected with the same plasma that was depleted of LOX or plasma at baseline (before surgery). Taken together, in addition to the known metastatic effects of LOX (Barker et al., 2012), our study reveals that LOX induction contributes to the rapid formation of a permissive niche for metastatic cell seeding in response to surgery.

EXPERIMENTAL PROCEDURES

Cell Lines

Murine Lewis lung carcinoma (LLC), EMT/6 and 4T1 mammary adenocarcinoma, and human MCF7 breast carcinoma cell lines were purchased from the American Type Culture Collection (ATCC). All cells were grown in DMEM, supplemented with 10% fetal calf serum, 1% L-glutamine, 1% sodium pyruvate, and 1% streptomycin, penicillin, and neomycin in solution (10 mg/mL, Biological Industries). Some of the cell lines (as indicated below) were stably transfected with GFP or mCherry vectors (Clontech Laboratories, 632379 and 631985, respectively). The cells were passaged in culture for no more than 4 months after being thawed from authentic stocks and were regularly tested and found to be mycoplasma-free.

Animal Tumor Models

The use of animals and experimental protocols were approved by the Animal Care and Use Committee of the Technion. BALB/c female mice (Harlan), 8–10 weeks of age, were orthotopically injected with 0.5×10^6 mCherry-expressing 4T1 (4T1-mCherry+) to the mammary fat pad. Tumor size was assessed regularly with Vernier calipers using the formula, $\text{width}^2 \times \text{length} \times 0.5$. An experimental pulmonary metastatic model was obtained using female BALB/c or C57BL/6 mice, 8–10 weeks of age, intravenously injected through the tail vein with 2.5×10^4 GFP-expressing EMT/6 (EMT/6-GFP+) or GFP-expressing LLC (LLC-GFP+) cells, respectively. Mouse survival was assessed daily. Mice were not randomized after surgery except in the case of the clinically relevant tumor model (4T1 mouse model). Mice were randomized in the case of plasma injection. The experiments were not blinded to the investigator; however, they were blinded to the mouse health care attendant who carried out daily health checks and reported on mice at endpoint. 10-week-old female $LOX^{-/+}$ C57BL/6 heterozygous mice described previously (Mäki et al., 2002) were used in some experiments. All in vivo and ex vivo experiments were repeated at least twice.

Surgical Procedures

Mice were anesthetized using an induction of 4% isoflurane, followed by maintenance anesthesia with 1.5% isoflurane. A sagittal cut through the abdominal cavity was performed using scalpel and scissors. A 1–1.5 cm incision in the peritoneum was then performed, followed by suturing with silk. For resection of primary 4T1 tumors, when tumors reached 150–200 mm^3, mice were anesthetized, and the mammary fat pad was exposed. Tumors were removed and the surgical area was subsequently sutured. Of note, all mice (control and surgery groups) received anesthesia and analgesic buprenorphine at a concentration of 0.04 mg/kg for three sequential days according to the institutional ethical protocols.

Plasma, Drugs, and Drug Concentrations

8- to 10-week-old BALB/c or C57Bl $LOX^{-/+}$ mice underwent the surgical procedure (as above) or left as control. After 24 hr, blood was drawn by cardiac puncture using citrate tubes, and plasma was separated. Plasma was injected intraperitoneally into recipient mice at a volume of 100 μL/mouse. In some

experiments, LOX was depleted from plasma as described in detail online. BAPN (Sigma-Aldrich) was injected intraperitoneally at a dose of 100 mg/kg daily for seven consecutive days, or as indicated in the text, as previously described (Bondareva et al., 2009). Rabbit anti-LOX antibodies were generated by GenScript against the EDTSCDYGYHRRFA peptide. The antibodies were intraperitoneally injected at a dose of 20 mg/kg as previously described (Erler et al., 2006). Control rabbit IgG antibodies (Jackson ImmunoResearch Laboratories) were injected intraperitoneally at a dose of 20 mg/kg. Recombinant LOX (OriGene) was injected intraperitoneally at a dose of 25 μg/kg, as previously described (Cox et al., 2015).

Human Plasma Samples

The human study was approved by the ethic committee at the European Institute of Oncology (EIO), Milan, Italy, and all patients signed an informed consent. Plasma from colorectal cancer patients, who underwent open abdominal surgery, was provided by the Department of Pathology at the EIO. Blood from the patients (n = 6) was collected at baseline (before surgery) and 24 hr after surgery. Plasma was separated and stored at −20°C until further use.

Flow Cytometry

Blood was drawn from anaesthetized mice by cardiac puncture and collected in EDTA tubes, and red blood cells were lysed. Lung samples or Matrigel plugs were prepared as single cell suspensions as previously described (Adini et al., 2009; Gingis-Velitski et al., 2011). CECs, CEPs, EMT/6-GFP, and 4T1-mCherry+ were analyzed by flow cytometry as previously described (Shaked et al., 2005). Details are provided in Supplemental Experimental Procedures.

Immunostaining

Frozen lung sections or Matrigel plugs were immunostained as previously described (Gingis-Velitski et al., 2011). Details are provided in Supplemental Experimental Procedures.

Focal Adhesion Assay

Plates coated with collagen (20 μg/mL), fibronectin (20 μg/mL), or laminin (20 μg/mL) were incubated with plasma from control, post-surgery mice or plasma from post-surgery mice depleted of LOX. After 4 hr, the plasma was washed and MCF7 cells (7×10^5/well) were seeded and cultured for 24 hr. MCF7 cells were then removed, and lysates were prepared to evaluate paxillin and p-pax expression by western blotting.

Ex Vivo PuMA

The assay was performed as previously described (Mendoza et al., 2010). Details are provided in Supplemental Experimental Procedures.

Collagen Assay

Collagen production in lung lysates was quantified using the SIRCOL Collagen Assay Kit (Biocolor) in accordance with the manufacturer's instructions. Details are provided in Supplemental Experimental Procedures.

Two-Photon Microscopy and Second Harmonics Generation and Quantification

To visualize ECM and collagen, a two-photon microscopy and a second harmonics generation system was used. Lungs from the different groups as indicated in the text were frozen in optimal cutting temperature (OCT) and sliced at a thickness of 150 μm in PBS. The slices were imaged using a two-photon microscope 2PM:Zeiss LSM 510 META NLO, equipped with a broadband Mai Tai-HP-femtosecond single box tunable Ti-sapphire oscillator, with automated broadband wavelength tuning 700–1,020 nm from Spectraphysics, for two-photon excitation. For second harmonic imaging (SHG) to detect collagen, a wavelength of 800 nm was used (detection at 400 nm). Images were acquired using the ×20 objective. Data were collected (n = 3 mice/group). For quantification measurements, images were analyzed using ImageJ 1.41k. To avoid edge effects (attenuation of the SHG signal at the top and bottom of the section), only the central image of each z stack was included in the quantification. Mean gray value limited to threshold of each image was calculated for each image and averaged over a set of at least five fields of view.

LOX Activity and Expression

LOX activity was evaluated as previously described (Siegel, 1974; Siegel et al., 1970). Briefly, a reaction solution containing 50 mM sodium borate (pH = 8.2) and 4 U/mL horseradish peroxidase was mixed with lung extracts to obtain a protein concentration of 250 μg/mL. The lysate extracts were obtained from mice treated with BAPN, anti-LOX, recombinant LOX, or rabbit polyclonal antibody using the same concentrations as above. Furthermore, lysate extracts of lungs or peritoneum obtained from control mice or mice that underwent surgery were treated with BAPN, anti-LOX antibodies, recombinant LOX, or rabbit polyclonal antibody and used as controls for the LOX activity assay. The enzymatic reaction was started by adding substrate mixture containing 50 mM sodium borate (pH = 8.2), 100 mM N-acetyl-3,7-dihydroxyphenoxazine (Amplex red; Molecular Probes, Invitrogen), and 20 mM 1,5-diaminopentane. In some experiments, 500 μM BAPN was added to the mixture as a negative inhibitory control. The production of H_2O_2 by LOX results in fluorescent resorfurin production, which can be measured (excitation at 540 nm and emission at 580 nm wavelengths). The fluorescent reaction was measured every 5 min for 1.5 hr at 37°C using a Fluorimeter (Fluo Star Galaxy). A representative plot out of three biological replicates was provided.

LOX expression in plasma and organ lysates (50 μg protein) was evaluated by ELISA (Cloud-Clone-Corp. SEC580Mu) in accordance with the manufacturer's instructions.

Oxidation Assay

To analyze the activity of LOX on different substrates, the oxidation assay was performed as previously described (Kraft-Sheleg et al., 2016; Zaffryar-Eilot et al., 2013). Briefly, the LOX activity assay was performed as above using lung lysates from control mice at a concentration of 200 μg/mL. The only modification is that the substrate (1,5-diaminopentane) used in the LOX activity assay was replaced with collagen (1 mg/mL), fibronectin (1 mg/mL), or laminin (1 mg/mL). The fluorescent reaction was measured every 5 min for 1.5 hr at 37°C using a Fluorimeter (Fluo Star Galaxy). A representative plot out of three biological replicates was provided.

Statistical Analysis

Data are expressed as mean ± SD. Statistical significance of the in vitro experiments was determined by either two-tailed Student's t test for a comparison between two groups or one-way ANOVA for multiple groups followed by Tukey ad hoc statistical test using GraphPad Prism 5.0. For the LOX activity assay and human experiment results, a comparison between control/baseline and the related group was calculated based on paired Student's t test. The number of replicates for each experiment is provided in Supplemental Information and/or figure legends. In the in vitro experiments, estimate of variance was performed and parameters for the statistical test were adjusted accordingly. In the in vivo/ex vivo studies, n = 3–7 mice/group (as specified in the figures) was used to reach statistical significance. The sample size for each experiment was designed to have 80% power at a two-sided α of 0.05. For the calculation of mouse survival, a Kaplan-Meier survival curve statistical analysis was performed in which the uncertainty of the fractional survival of 95% confidence intervals was calculated. Differences between all groups were compared and were considered significant at values below 0.05.

SUPPLEMENTAL INFORMATION

Supplemental Information includes Supplemental Experimental Procedures and six figures and can be found with this article online at http://dx.doi.org/10.1016/j.celrep.2017.04.005.

AUTHOR CONTRIBUTIONS

C.R.-T., P.H., and Y.S. conceived and designed all experiments. Experiments were performed by C.R.-T. with the assistance of S.Z.-E., M.G., and M.T.; J.M.M. and J.M. provided LOX mutant mice. D.R. and F.B. provided human samples. F.B., I.S., D.H., P.H., and Y.S. discussed and analyzed the data. P.H. and Y.S. supervised the overall project. C.R.-T., P.H., and Y.S. wrote the manuscript.

ACKNOWLEDGMENTS

We would like to thank Dr. V. Kalchenko for technical assistance with the two-photon microscope. This work is primarily supported by the European Research Council (grant 260633, Y.S.) and Rappaport Institute (Y.S. and P.H.) J.M. was supported by the Academy of Finland Center of Excellence (grant 251314), the S. Juselius Foundation, and the Jane and Aatos Erkko Foundation. F.B. is supported by Associazione Italiana per la Ricerca sul Cancro (AIRC).

Received: October 1, 2016
Revised: February 27, 2017
Accepted: March 24, 2017
Published: April 25, 2017

REFERENCES

Adini, A., Fainaru, O., Udagawa, T., Connor, K.M., Folkman, J., and D'Amato, R.J. (2009). Matrigel cytometry: a novel method for quantifying angiogenesis in vivo. J. Immunol. Methods *342*, 78–81.

Ando, N., Iizuka, T., Ide, H., Ishida, K., Shinoda, M., Nishimaki, T., Takiyama, W., Watanabe, H., Isono, K., Aoyama, N., et al.; Japan Clinical Oncology Group (2003). Surgery plus chemotherapy compared with surgery alone for localized squamous cell carcinoma of the thoracic esophagus: a Japan Clinical Oncology Group Study–JCOG9204. J. Clin. Oncol. *21*, 4592–4596.

Baker, A.M., Bird, D., Welti, J.C., Gourlaouen, M., Lang, G., Murray, G.I., Reynolds, A.R., Cox, T.R., and Erler, J.T. (2013). Lysyl oxidase plays a critical role in endothelial cell stimulation to drive tumor angiogenesis. Cancer Res. *73*, 583–594.

Barcellos-Hoff, M.H., Park, C., and Wright, E.G. (2005). Radiation and the microenvironment - tumorigenesis and therapy. Nat. Rev. Cancer *5*, 867–875.

Barker, H.E., Cox, T.R., and Erler, J.T. (2012). The rationale for targeting the LOX family in cancer. Nat. Rev. Cancer *12*, 540–552.

Beyar-Katz, O., Magidey, K., Ben-Tsedek, N., Alishekevitz, D., Timaner, M., Miller, V., Lindzen, M., Yarden, Y., Avivi, I., and Shaked, Y. (2016). Bortezomib-induced pro-inflammatory macrophages as a potential factor limiting anti-tumour efficacy. J. Pathol. *239*, 262–273.

Blagosklonny, M.V. (2001). Hypoxia-inducible factor: Achilles' heel of antiangiogenic cancer therapy (review). Int. J. Oncol. *19*, 257–262.

Bondareva, A., Downey, C.M., Ayres, F., Liu, W., Boyd, S.K., Hallgrimsson, B., and Jirik, F.R. (2009). The lysyl oxidase inhibitor, beta-aminopropionitrile, diminishes the metastatic colonization potential of circulating breast cancer cells. PLoS ONE *4*, e5620.

Bono, A., Bianchi, P., Locatelli, A., Calleri, A., Quarna, J., Antoniott, P., Rabascio, C., Mancuso, P., Andreoni, B., and Bertolini, F. (2010). Angiogenic cells, macroparticles and RNA transcripts in laparoscopic vs open surgery for colorectal cancer. Cancer Biol. Ther. *10*, 682–685.

Ceelen, W., Pattyn, P., and Mareel, M. (2014). Surgery, wound healing, and metastasis: recent insights and clinical implications. Crit. Rev. Oncol. Hematol. *89*, 16–26.

Coffey, J.C., Wang, J.H., Smith, M.J., Bouchier-Hayes, D., Cotter, T.G., and Redmond, H.P. (2003). Excisional surgery for cancer cure: therapy at a cost. Lancet Oncol. *4*, 760–768.

Cox, T.R., Bird, D., Baker, A.M., Barker, H.E., Ho, M.W., Lang, G., and Erler, J.T. (2013). LOX-mediated collagen crosslinking is responsible for fibrosis-enhanced metastasis. Cancer Res. *73*, 1721–1732.

Cox, T.R., Rumney, R.M., Schoof, E.M., Perryman, L., Høye, A.M., Agrawal, A., Bird, D., Latif, N.A., Forrest, H., Evans, H.R., et al. (2015). The hypoxic cancer secretome induces pre-metastatic bone lesions through lysyl oxidase. Nature *522*, 106–110.

Daenen, L.G., Roodhart, J.M., van Amersfoort, M., Dehnad, M., Roessingh, W., Ulfman, L.H., Derksen, P.W., and Voest, E.E. (2011). Chemotherapy enhances metastasis formation via VEGFR-1-expressing endothelial cells. Cancer Res. *71*, 6976–6985.

Decitre, M., Gleyzal, C., Raccurt, M., Peyrol, S., Aubert-Foucher, E., Csiszar, K., and Sommer, P. (1998). Lysyl oxidase-like protein localizes to sites of de novo fibrinogenesis in fibrosis and in the early stromal reaction of ductal breast carcinomas. Lab. Invest. *78*, 143–151.

DeLisser, H.M., Keirns, C.C., Clinton, E.A., and Margolis, M.L. (2009). "The air got to it:" exploring a belief about surgery for lung cancer. J. Natl. Med. Assoc. *101*, 765–771.

Demicheli, R., Abbattista, A., Miceli, R., Valagussa, P., and Bonadonna, G. (1996). Time distribution of the recurrence risk for breast cancer patients undergoing mastectomy: further support about the concept of tumor dormancy. Breast Cancer Res. Treat. *41*, 177–185.

Demicheli, R., Retsky, M.W., Hrushesky, W.J., Baum, M., and Gukas, I.D. (2008). The effects of surgery on tumor growth: a century of investigations. Ann. Oncol. *19*, 1821–1828.

Ebos, J.M., Lee, C.R., Cruz-Munoz, W., Bjarnason, G.A., Christensen, J.G., and Kerbel, R.S. (2009). Accelerated metastasis after short-term treatment with a potent inhibitor of tumor angiogenesis. Cancer Cell *15*, 232–239.

Erler, J.T., Bennewith, K.L., Nicolau, M., Dornhöfer, N., Kong, C., Le, Q.T., Chi, J.T., Jeffrey, S.S., and Giaccia, A.J. (2006). Lysyl oxidase is essential for hypoxia-induced metastasis. Nature *440*, 1222–1226.

Erler, J.T., Bennewith, K.L., Cox, T.R., Lang, G., Bird, D., Koong, A., Le, Q.T., and Giaccia, A.J. (2009). Hypoxia-induced lysyl oxidase is a critical mediator of bone marrow cell recruitment to form the premetastatic niche. Cancer Cell *15*, 35–44.

Gingis-Velitski, S., Loven, D., Benayoun, L., Munster, M., Bril, R., Voloshin, T., Alishekevitz, D., Bertolini, F., and Shaked, Y. (2011). Host response to short-term, single-agent chemotherapy induces matrix metalloproteinase-9 expression and accelerates metastasis in mice. Cancer Res. *71*, 6986–6996.

Heino, J., and Käpylä, J. (2009). Cellular receptors of extracellular matrix molecules. Curr. Pharm. Des. *15*, 1309–1317.

Hofer, S.O., Molema, G., Hermens, R.A., Wanebo, H.J., Reichner, J.S., and Hoekstra, H.J. (1999). The effect of surgical wounding on tumour development. Eur. J. Surg. Oncol. *25*, 231–243.

James, A., Daley, C.M., and Greiner, K.A. (2011). "Cutting" on cancer: attitudes about cancer spread and surgery among primary care patients in the U.S.A. Soc. Sci. Med. *73*, 1669–1673.

Kaplan, R.N., Riba, R.D., Zacharoulis, S., Bramley, A.H., Vincent, L., Costa, C., MacDonald, D.D., Jin, D.K., Shido, K., Kerns, S.A., et al. (2005). VEGFR1-positive haematopoietic bone marrow progenitors initiate the pre-metastatic niche. Nature *438*, 820–827.

Kraft-Sheleg, O., Zaffryar-Eilot, S., Genin, O., Yaseen, W., Soueid-Baumgarten, S., Kessler, O., Smolkin, T., Akiri, G., Neufeld, G., Cinnamon, Y., and Hasson, P. (2016). Localized LoxL3-dependent fibronectin oxidation regulates myofiber stretch and integrin-mediated adhesion. Dev. Cell *36*, 550–561.

Larsen, M., Artym, V.V., Green, J.A., and Yamada, K.M. (2006). The matrix reorganized: extracellular matrix remodeling and integrin signaling. Curr. Opin. Cell Biol. *18*, 463–471.

Mäki, J.M., Räsänen, J., Tikkanen, H., Sormunen, R., Mäkikallio, K., Kivirikko, K.I., and Soininen, R. (2002). Inactivation of the lysyl oxidase gene Lox leads to aortic aneurysms, cardiovascular dysfunction, and perinatal death in mice. Circulation *106*, 2503–2509.

Mendoza, A., Hong, S.H., Osborne, T., Khan, M.A., Campbell, K., Briggs, J., Eleswarapu, A., Buquo, L., Ren, L., Hewitt, S.M., et al. (2010). Modeling metastasis biology and therapy in real time in the mouse lung. J. Clin. Invest. *120*, 2979–2988.

Minsky, B.D., Mies, C., Rich, T.A., Recht, A., and Chaffey, J.T. (1988). Potentially curative surgery of colon cancer: patterns of failure and survival. J. Clin. Oncol. *6*, 106–118.

Pàez-Ribes, M., Allen, E., Hudock, J., Takeda, T., Okuyama, H., Viñals, F., Inoue, M., Bergers, G., Hanahan, D., and Casanovas, O. (2009). Antiangiogenic therapy elicits malignant progression of tumors to increased local invasion and distant metastasis. Cancer Cell *15*, 220–231.

Paraskeva, P.A., Ridgway, P.F., Olsen, S., Isacke, C., Peck, D.H., and Darzi, A.W. (2006). A surgically induced hypoxic environment causes changes in the metastatic behaviour of tumours in vitro. Clin. Exp. Metastasis *23*, 149–157.

Psaila, B., Kaplan, R.N., Port, E.R., and Lyden, D. (2006). Priming the 'soil' for breast cancer metastasis: the pre-metastatic niche. Breast Dis. *26*, 65–74.

Rahbari, N.N., Kedrin, D., Incio, J., Liu, H., Ho, W.W., Nia, H.T., Edrich, C.M., Jung, K., Daubriac, J., Chen, I., et al. (2016). Anti-VEGF therapy induces ECM remodeling and mechanical barriers to therapy in colorectal cancer liver metastases. Sci. Transl. Med. *8*, 360ra135.

Retsky, M., Rogers, R., Demicheli, R., Hrushesky, W.J., Gukas, I., Vaidya, J.S., Baum, M., Forget, P., Dekock, M., and Pachmann, K. (2012). NSAID analgesic ketorolac used perioperatively may suppress early breast cancer relapse: particular relevance to triple negative subgroup. Breast Cancer Res. Treat. *134*, 881–888.

Semenza, G.L. (2012). Hypoxia-inducible factors: mediators of cancer progression and targets for cancer therapy. Trends Pharmacol. Sci. *33*, 207–214.

Shaked, Y. (2016). Balancing efficacy of and host immune responses to cancer therapy: the yin and yang effects. Nat. Rev. Clin. Oncol. *13*, 611–626.

Shaked, Y., Bertolini, F., Man, S., Rogers, M.S., Cervi, D., Foutz, T., Rawn, K., Voskas, D., Dumont, D.J., Ben-David, Y., et al. (2005). Genetic heterogeneity of the vasculogenic phenotype parallels angiogenesis; Implications for cellular surrogate marker analysis of antiangiogenesis. Cancer Cell *7*, 101–111.

Shchors, K., Nozawa, H., Xu, J., Rostker, F., Swigart-Brown, L., Evan, G., and Hanahan, D. (2013). Increased invasiveness of MMP-9-deficient tumors in two mouse models of neuroendocrine tumorigenesis. Oncogene *32*, 502–513.

Siegel, R.C. (1974). Biosynthesis of collagen crosslinks: increased activity of purified lysyl oxidase with reconstituted collagen fibrils. Proc. Natl. Acad. Sci. USA *71*, 4826–4830.

Siegel, R.C., Pinnell, S.R., and Martin, G.R. (1970). Cross-linking of collagen and elastin. Properties of lysyl oxidase. Biochemistry *9*, 4486–4492.

Takemoto, Y., Li, T.S., Kubo, M., Ohshima, M., Kurazumi, H., Ueda, K., Enoki, T., Murata, T., and Hamano, K. (2012). The mobilization and recruitment of c-kit+ cells contribute to wound healing after surgery. PLoS ONE *7*, e48052.

Timaner, M., Bril, R., Kaidar-Person, O., Rachman-Tzemah, C., Alishekevitz, D., Kotsofruk, R., Miller, V., Nevelsky, A., Daniel, S., Raviv, Z., et al. (2015). Dequalinium blocks macrophage-induced metastasis following local radiation. Oncotarget *6*, 27537–27554.

Turner, C.E., Glenney, J.R., Jr., and Burridge, K. (1990). Paxillin: a new vinculin-binding protein present in focal adhesions. J. Cell Biol. *111*, 1059–1068.

van der Bij, G.J., Oosterling, S.J., Beelen, R.H., Meijer, S., Coffey, J.C., and van Egmond, M. (2009). The perioperative period is an underutilized window of therapeutic opportunity in patients with colorectal cancer. Ann. Surg. *249*, 727–734.

Zaffryar-Eilot, S., Marshall, D., Voloshin, T., Bar-Zion, A., Spangler, R., Kessler, O., Ghermazien, H., Brekhman, V., Suss-Toby, E., Adam, D., et al. (2013). Lysyl oxidase-like-2 promotes tumour angiogenesis and is a potential therapeutic target in angiogenic tumours. Carcinogenesis *34*, 2370–2379.

Zaidel-Bar, R., Milo, R., Kam, Z., and Geiger, B. (2007). A paxillin tyrosine phosphorylation switch regulates the assembly and form of cell-matrix adhesions. J. Cell Sci. *120*, 137–148.

Cell Reports, Volume *19*

Supplemental Information

Blocking Surgically Induced Lysyl Oxidase Activity Reduces the Risk of Lung Metastases

Chen Rachman-Tzemah, Shelly Zaffryar-Eilot, Moran Grossman, Dario Ribero, Michael Timaner, Joni M. Mäki, Johanna Myllyharju, Francesco Bertolini, Dov Hershkovitz, Irit Sagi, Peleg Hasson, and Yuval Shaked

Supplemental Online Materials

Supplemental Experimental Procedures

Flow cytometry

Blood was drawn from anaesthetized mice by cardiac puncture, collected in EDTA tubes and red blood cells were lysed. Lung samples or Matrigel plugs were prepared as single cell suspensions as previously described (Adini et al., 2009; Gingis-Velitski et al., 2011). Viable circulating endothelial cells (CEC), endothelial progenitor cells (CEPs), and endothelial cells were quantified by flow cytometry using the following surface markers: for CECs, CD45-/VEGFR2+; for CEPs, CD13+/VEGFR2+/CD117+/CD45-; and for endothelial cells, CD45-/VEGFR2+/CD31+. All antibodies were purchased from BioLegend or BD biosciences, using the following clones: CD45 (30-F11); CD13 (R3-242); VEGFR2 (89B3A5); CD117 (ACK2); and CD31 (390). In some experiments GFP+ EMT/6 or mCherry+ 4T1 cells colonizing the lungs were quantified. Analyses were performed using CyAn Flow cytometer. At least 100,000 cells per sample were acquired. Analyses were considered informative when an adequate number of events (ie >25, typically 50 -150) were collected in the appropriate enumeration gates of samples from untreated control mice. Percentages of stained cells were determined and compared to appropriate negative controls. Positive staining was defined as being greater than non-specific background staining, and 7-aminoactinomycin D (7AAD) was used to distinguish apoptotic and dead cells from viable cells (Philpott et al., 1996).

Immunostaining

Frozen lung sections or Matrigel plugs were immunostained as previously described (Gingis-Velitski et al., 2011). Briefly, endothelial cells in Matrigel plugs were stained with anti-CD31 antibody (1:100, BD Biosciences). LOX expression in lung sections was evaluated using rabbit anti-LOX antibody as previously described (Erler et al., 2006). Cy3-conjugated and DyLight-488-conjugated secondary antibodies were used (1:200, Jackson ImmunoResearch). In some experiments, lungs were embedded in paraffin. Lung sections were immunostained with LOX (as above) followed by histidine peroxidase anti-mouse and anti-rabbit secondary antibodies (Nichirei, Japan). Staining was developed using AEC simple stain solution (Nichirei). Hematoxylin (Sigma) was used as a counterstain. Polyclonal rabbit anti-Phospho-Paxillin (1:100, Cell signaling, 2541), and a secondary mouse-anti rabbit Cy3-conjugated antibody (1:200, Jackson ImmunoResearch) were used. Nuclei were stained with 6-diamidino-2-phenylindole (DAPI). Immunostaining for hypoxia was performed using Hypoxyprobe-1 (Chemicon International, Temecula, CA) according to the manufacturer's instructions, and as previously described in (Shaked et al., 2006). Briefly, mice received an IP injection of pimonidazole hydrochloride (60mg/kg) 90

min before euthanasia. Peritoneum cryosection immunostaining was performed using anti-pimonidazole antibody (1:200) and its secondary Cy3-conjugated rat anti-mouse antibody (1:200, Jackson ImmunoResearch Laboratories Inc.). Images were captured using the Leica CTR 6000 system unless otherwise indicated.

Depletion of LOX from plasma

Neutralizing antibodies for LOX (10 µg/ml) were generated by GenScript against the EDTSCDYGYHRRFA peptide. Anti-LOX antibodies (1 µg) were added to 500 µl plasma obtained from BALB/c control mice, mice that underwent surgery, or pooled plasma samples from patients (n=6) at baseline or 24 hours post-surgery. The mix was incubated for 1 hour with rotation at 4^{o}C. Antibodies were then depleted from the plasma using a mix of protein A/G sepharose beads (Abcam, ab193262). LOX depletion was verified by ELISA (Cloud-Clon-Corp., SEC580Mu), in accordance with the manufacturer's instructions. Subsequently, plasma was injected into naive BALB/c mice as described in the text.

Ex vivo pulmonary metastatic assay (PuMA)

The assay was performed as previously described (Mendoza et al., 2010). Briefly, EMT/6-GFP+ cells (2.5×10^4) were injected to mice via the tail vein. Fifteen minutes later, mice were anesthetized, and the trachea was cannulated with a 21G intravenous catheter and attached to a gravity perfusion apparatus. The lungs were filled in the vertical position with heated agarose medium solution containing M-199 media, sodium bicarbonate, hydrocortisone, bovine insulin, penicillin/streptomycin and agarose. The ratio of agarose to medium was 1:1 (w/v). The lungs were then removed and placed in cold PBS. Transverse serial sections (1-2mm in thickness) were gently sliced from each lobe with a scalpel and incubated on Matrigel covered plates for 6 days at 37°C. The lung slices were then analyzed for GFP+ cells using Olympus SZX9 fluorescence stereo microscope or Leica CTR 6000 microscope system.

Collagen assay

Collagen production in lung lysates was quantified using the SIRCOL Collagen Assay Kit (Biocolor, Belfast, UK) in accordance with the manufacturer's instructions. Briefly, SIRCOL dye reagent was added to lung extracts followed by agitation in a mechanical shaker for 30 minutes. The collagen-dye complexes were pelleted by centrifugation at 12,000g for 10 minutes. The pellet was washed with acid-salt wash-reagent and centrifuged again at 12,000g for 10 minutes. Alkali reagent was then added to the samples, standards and blanks. Absorption at 555 nm was measured using a spectrophotometer, and collagen

concentration was calculated according to the standard curve. Results were normalized according to the protein concentration in lung extracts. The experiment was performed in triplicate.

Aortic ring assay

The aortic ring assay was performed by dissecting 1mm long aortic rings from non-tumor bearing BALB/c mice, as previously described (Gingis-Velitski et al., 2011). The aortic ring was embedded in Matrigel (BD Bioscience), and then cultured for 10 days in DMEM supplemented with 10% plasma from control mice or 24 hours after mice underwent surgery. Plasma-containing medium was replaced every 3 days. Sprouting microvessels in the Matrigel-embedded aortic ring were visualized by light-microscopy using the Leica CTR 6000 system.

Tube forming assay

Tube forming assay was carried out in 48 well plates pre-coated with 150µl of Matrigel. HUVEC cells ($2x10^5$, purchased from LONZA, Switzerland) were seeded in each well and incubated for 12hr with M-199 medium containing 10% plasma from control mice or mice that underwent surgery. Microtubes formed by the HUVECs were analyzed using Time Lapse Microscopy by Zeiss Axio observer system. The number of bifurcations was counted per field, and then plotted. The experiment was performed in triplicate.

Matrigel plug assay

The evaluation of host cells colonizing Matrigel plugs was performed as previously described (Gingis-Velitski et al., 2011). Briefly, 50 µl plasma from control mice or from mice 24 hours after they underwent surgery were added to 0.5ml Matrigel (ratio of 1:10). Subsequently, Matrigel was implanted into both flanks of 8-10 week-old BALB/c mice to create plugs. After 10 days, plugs were removed and either sectioned or prepared as single cell suspensions. Frozen sections were immunostained for endothelial cells (as described below). Images were captured using Leica CTR 6000 system.

Evans Blue permeabilization assay

Lung vascular permeability was performed using Evans blue assay as previously described (Hiratsuka et al., 2011). Briefly, control or post-surgery (24 hours) mice were intravenously injected with Evans blue solution (100µl/mouse, 4mg/ml PBS). After 2 hours, mice were perfused with PBS and subsequently lungs were removed and imaged. Lungs were homogenized in PBS (100mg tissue/ml) and incubated in formamide (2mg/100mg tissue) at 60^0C overnight. Evans blue absorption in tissue was evaluated using

ELISA reader (TECAN infinite M200Pro) with absorbance at 620nm and 740nm wavelengths, as previously described (Hiratsuka et al., 2011).

Western blot

MCF7 cell lysates were subjected to SDS-PAGE. Proteins were electro-transferred to nitrocellulose membranes, which were then probed with polyclonal rabbit anti-paxillin (1:1000; Cell Signaling, 2542) and anti-phospho-paxillin (1:1000; Cell Signaling, 2541), or anti-α tubulin (1:1000, Abcam, Ab4074). For the detection of p-pax, cells were lysed in Hepes 50 mM PH-7.5, EDTA 4 mM, Triton 1%, 0.5 mg/ml Na3VO4, 4.5 mg/ml Na2P2O7.

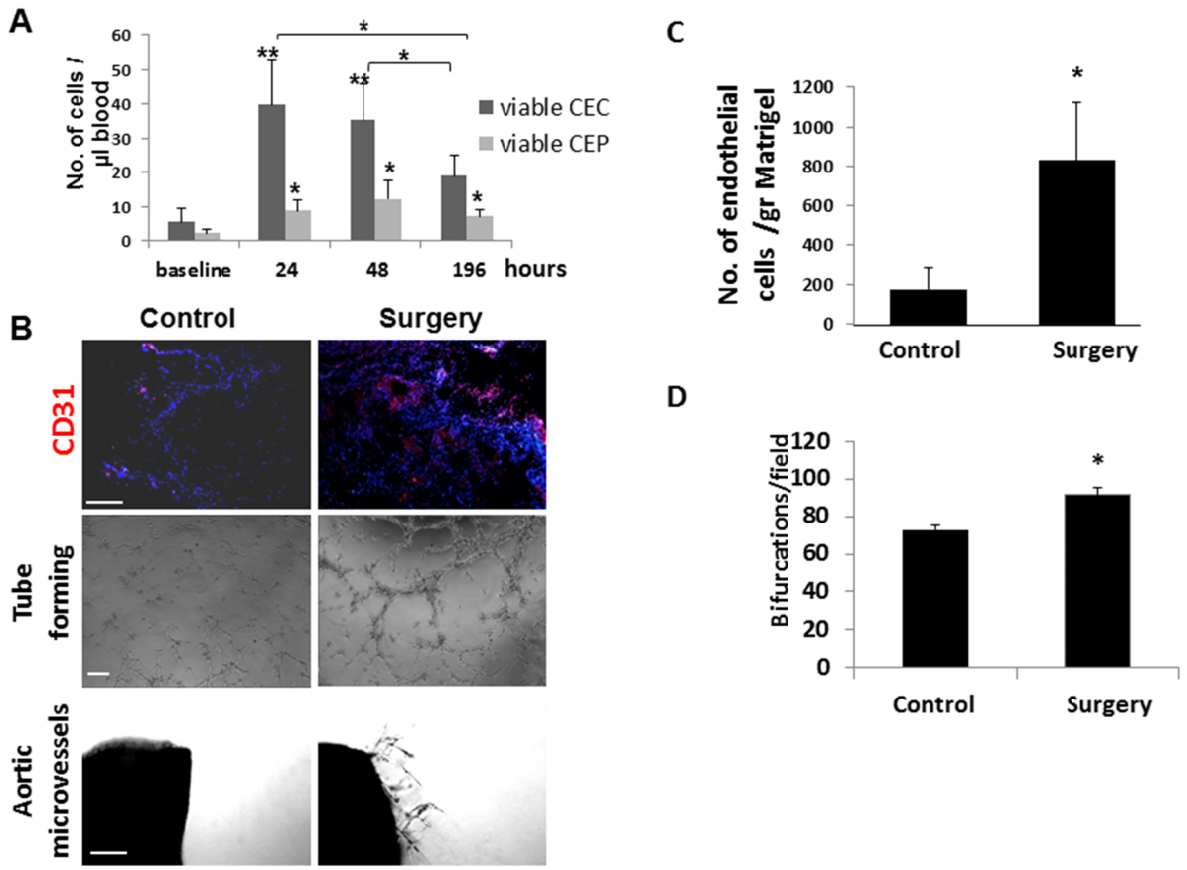

Figure S1 (related to Figure 1): Increased systemic and local angiogenesis in mice that undergo surgery. (A) Abdominal surgery was performed on 8-10 week old non-tumor bearing BALB/c mice (n=5). Blood was drawn from the retro-orbital sinus at several time points following surgery as indicated, and subsequently assessed for levels of viable CECs and viable CEPs. *p<0.05; **p<0.01; ***p<0.001 using one way ANOVA followed by Tukey post-hoc test. (B) Upper panel: Plasma obtained from control or post-surgery mice was added to Matrigel in a 1:10 ratio. The Matrigel was implanted into the flanks of mice (n=5 mice/group), and plugs were removed after 10 days and sectioned. Sections were stained for endothelial cells using anti-CD31 antibodies (red). Nuclei were stained with DAPI (blue). Middle panel: HUVECs cultured on Matrigel-coated plates for 12 hours in the presence of 10% plasma drawn from control and post-surgery mice. Microvessel tube formation (n=3/group) was assessed. Lower panel: Matrigel-embedded aortic rings (n=4/group) were incubated with medium containing 10 % plasma from control and post-surgery mice. Microvessel sprouting was analyzed using Leica CTR 6000 system. Images were captured with the Leica CTR 6000 system. Representative images are shown. Scale bar= 200µm. (C) The number of endothelial cells in Matrigel (B) was quantified by preparing single cell suspensions that were immunostained with CD31 (endothelial cell marker) and assessed by flow cytometry. (D) The number of bifurcations of HUVEC tube forming assay (B) were quantified. *p<0.05, as assessed by two-tailed Student's t-test.

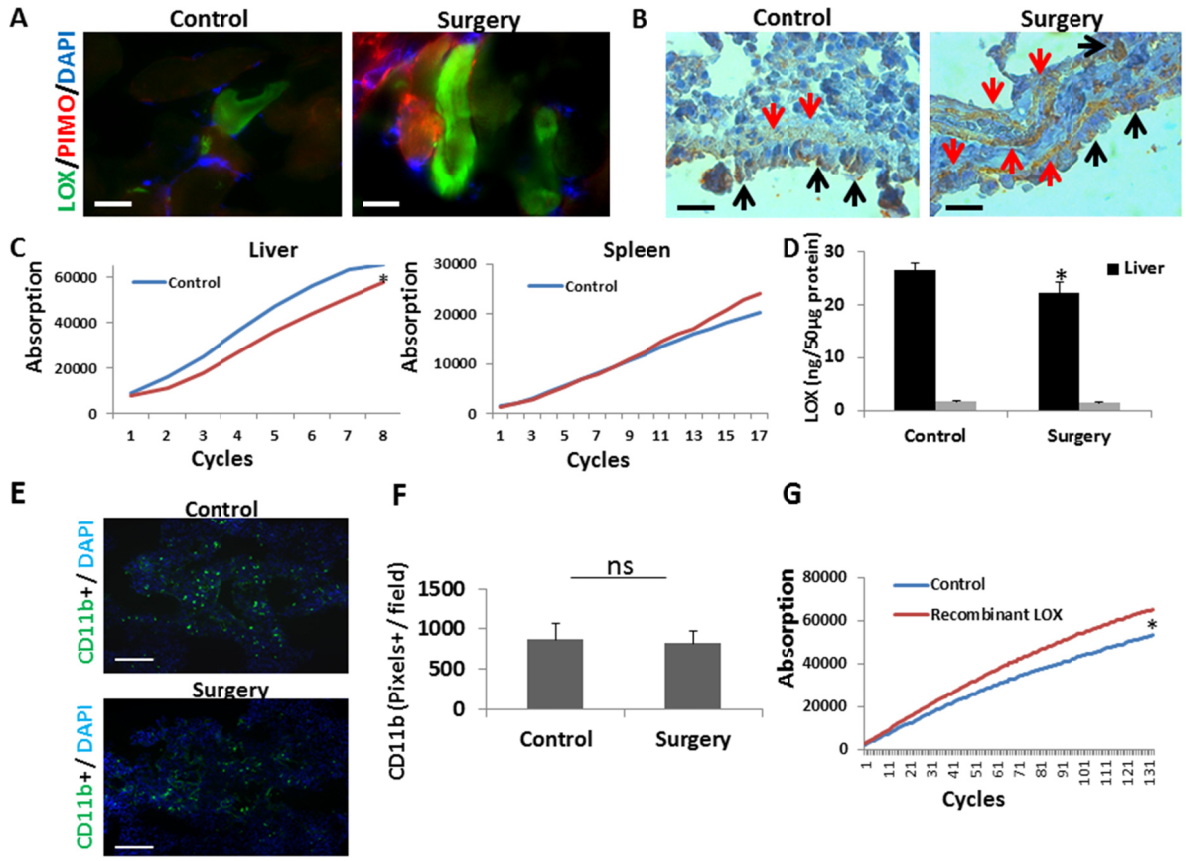

Figure S2 (related to Figure 2): LOX activity and expression in organs as well as CD11b colonization of lungs from mice that undergo surgery. (A-B) A 1 cm incision in the abdomen of non-tumor bearing 8-10 week old BALB/c mice was performed. Control mice have not undergone any surgical procedure (n=3-5 mice /group). After 24 hours, mice were sacrificed, and peritoneum and lungs were removed. (A) High magnification images of immunostained peritoneum from control or post-surgery mice. LOX and pimonidazole marking hypoxia are designated in green and red, respectively. Nuclei were stained with DAPI (blue). Scale bar=20µm. (B) Lung paraffin sections were immunostained for LOX (brown). Counterstaining was performed using hematoxylin. Images were taken in x1000 magnification. Extracellular and intracellular LOX immunostainings are indicated in red and black arrows, respectively. Scale bar=20µm. (C-D) Eight-to-ten week old BALB/c control or 24 hours post-surgery mice (n=3 mice/group) were sacrificed and organs such as liver and spleen were harvested. Lysates of liver and spleen were assessed for LOX activity (C) or LOX expression (D). LOX activity was assessed by paired Student's t-test. A representative graph from three biological replicates is provided. (E-F) Eight-to-ten week old BALB/c mice underwent surgery or were left as controls (n=4 mice/group). Three days later, the mice were sacrificed and the lungs were removed. Lungs sections were immunostained for CD11b (green). DAPI was used for counterstaining (blue). (E) Representative images of lung sections stained with CD11b are provided. Scale bar= 200µm. (F) The number of positive pixels for CD11b from each field was quantified using Photoshop 6 (n=20 fields/group). (G) Lysates of control lungs were assessed for LOX activity after the mice were treated with recombinant LOX or PBS (Control). *$p<0.05$, or non-significant (ns) as assessed by two-tailed Student's t-test.

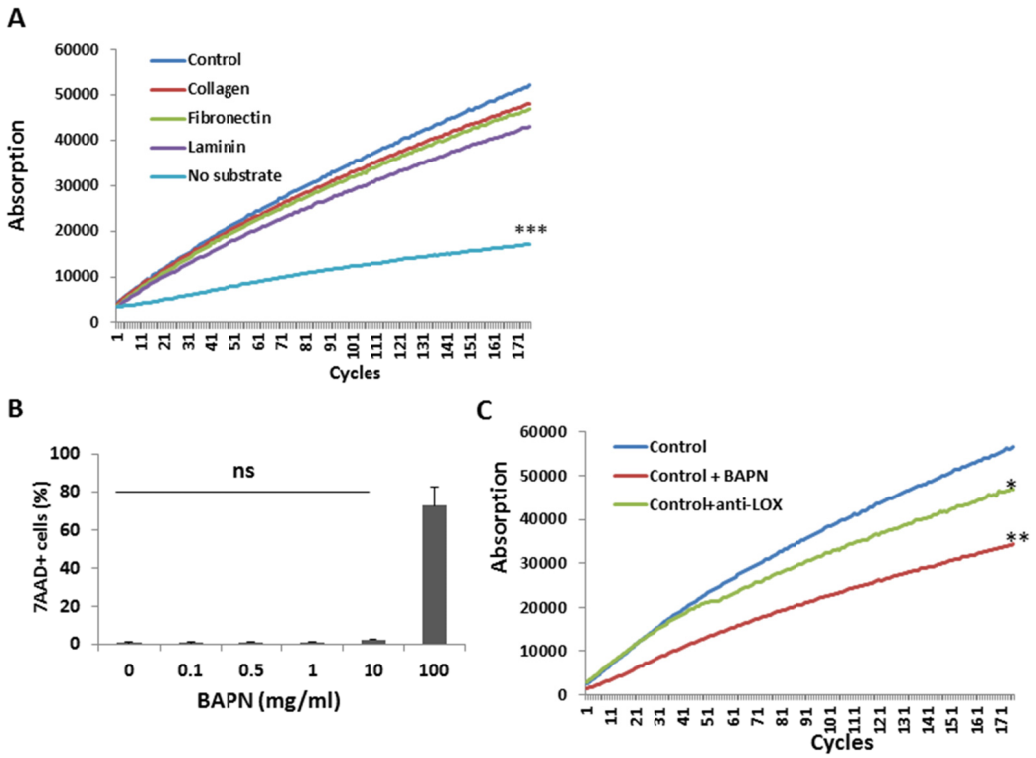

Figure S3 (related to Figures 3-4): LOX activity in different conditions. (A) Lysates of control lungs were used in an oxidation assay in which the substrate was replaced by collagen, fibronectin or laminin. 1,5-diaminopentane was used as a positive control (Control), while no substrate was used as a negative control. (B) EMT/6 cells were cultured in the presence of escalating doses of BAPN as indicated. After 24 hours in culture, cells were analyzed by flow cytometry for the percentage of 7AAD+ cells. Three biological replicates were carried out and results were plotted. Results did not reach statistical significance (ns) at a dose range of 0-10mg/ml, as assessed by one way ANOVA followed by Tukey post-hoc test. (C) Lysates of lungs from post-surgery mice treated with BAPN (100mg/kg) or anti-LOX antibodies (20mg/kg) were assessed for LOX activity. LOX activity in all experiments was assessed by two-tailed Student's t-test. A representative graph from three biological replicates is provided. *$p<0.05$; **$p<0.01$; using Student's t-test.

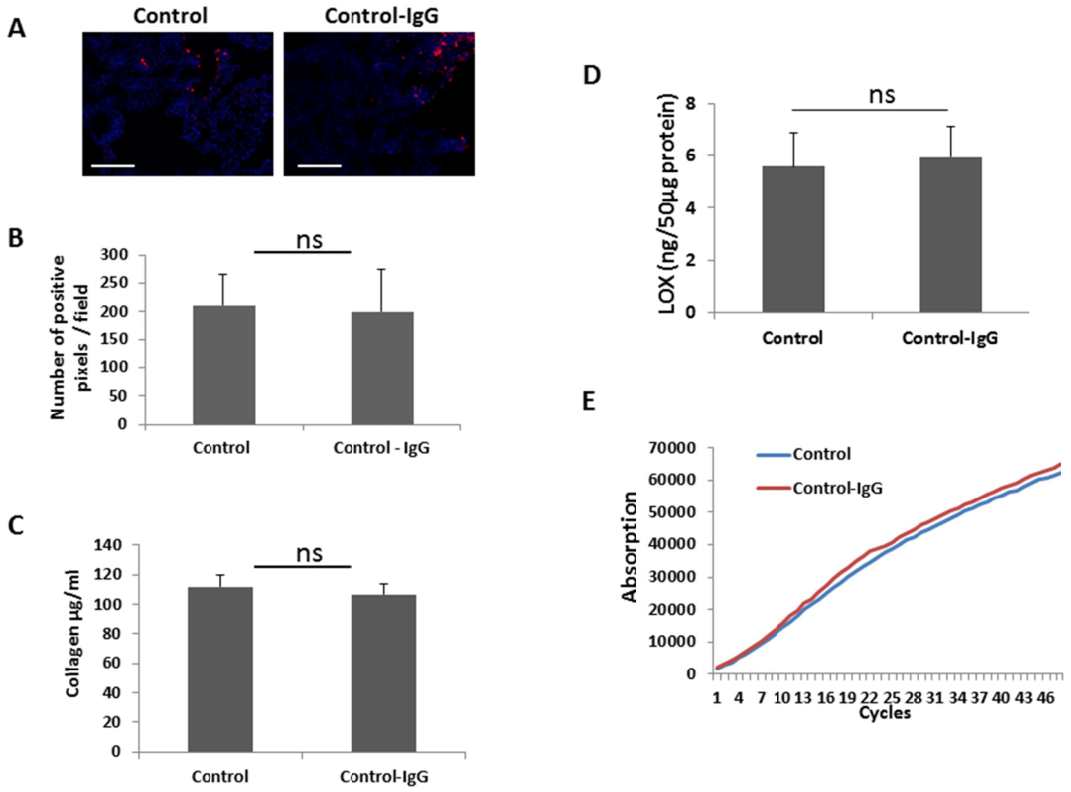

Figure S4 (related to Figure 4): LOX expression and activity in the lungs of mice treated with rabbit IgG. Eight-to-ten week old BALB/c mice (n=3 mice/group) were left untreated (control) or injected with 20mg/kg rabbit IgG. After 3 days, lungs were removed. (A) Lung sections were immunostained for LOX (red). Representative images are provided. Scale bar=200µm. (B) LOX positive pixels (from A) were calculated per field (n=15 fields/group). (C-E) Lung lysates were assessed for newly synthesized collagen (C) LOX expression (D) and LOX activity (E). Representative graph for LOX activity is provided from 3 biological replicates. Non-significant (ns) changes were found as assessed by two-tailed Student's t-test.

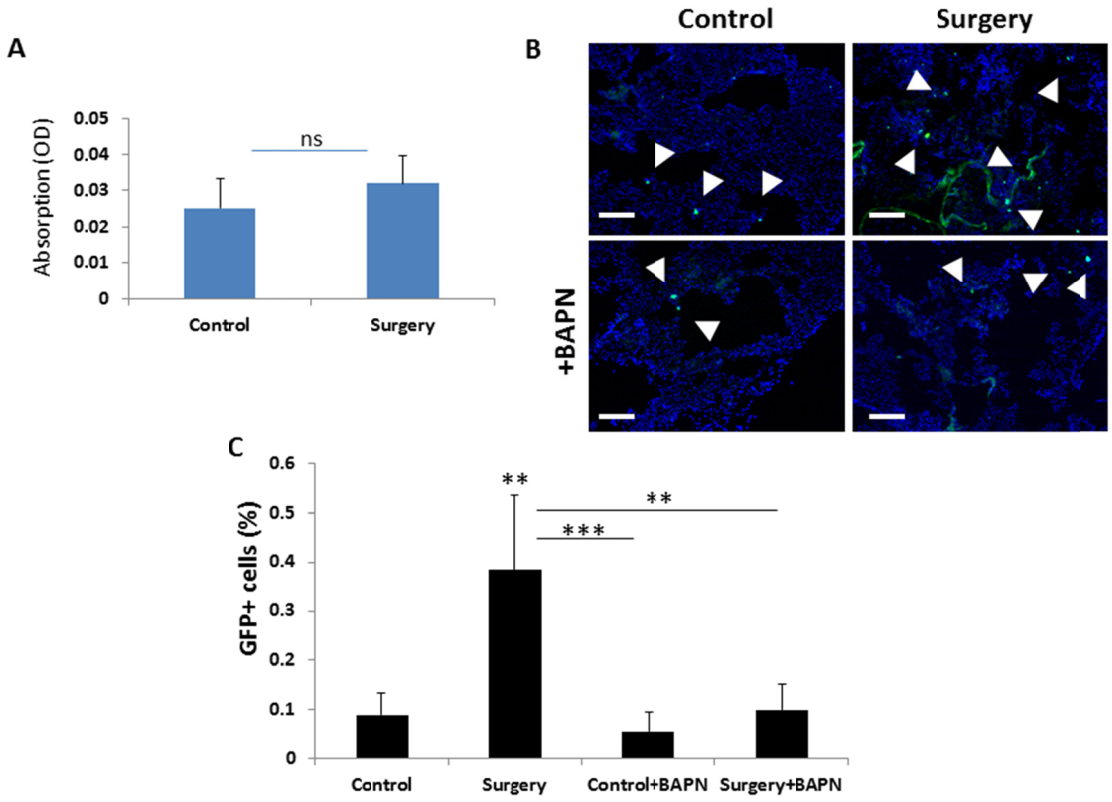

Figure S5 (related to Figure 4): Lung permeability and tumor cell seeding in control and post-surgery mice. (A) Eight-to-ten week old BALB/c mice (n=3/group) were left untreated or underwent abdominal surgery. After 24 hours, mice were injected with Evans blue to evaluate lung permeability, as described in Experimental procedures. Lung images were captured, and Evans blue absorption was quantified in lung lysates. ns – not significant. (B-C) Eight-to-ten week old BALB/c mice were treated with BAPN or PBS for 3 sequential days. After 24 hours, mice either underwent surgery or were left as controls (n=4 mice/group). After an additional 24 hours EMT/6-GFP+ cells ($2x10^5$/mouse) were injected through the tail vein. Twenty minutes later, mice were perfused with PBS and lungs were removed. (B) Lung cryosections were imaged under fluorescent microscope to evaluate the number of GFP+ cells (green) in the lungs. White arrows indicate GFP+ cells. Scale bar=200µm. (C) In a parallel experiment, lungs were removed and prepared as single cell suspensions. The percentage of GFP+ cells in the lungs was quantified by flow cytometry. **p<0.01; *** p<0.001 as assessed by one way ANOVA followed by Tukey post-hoc test.

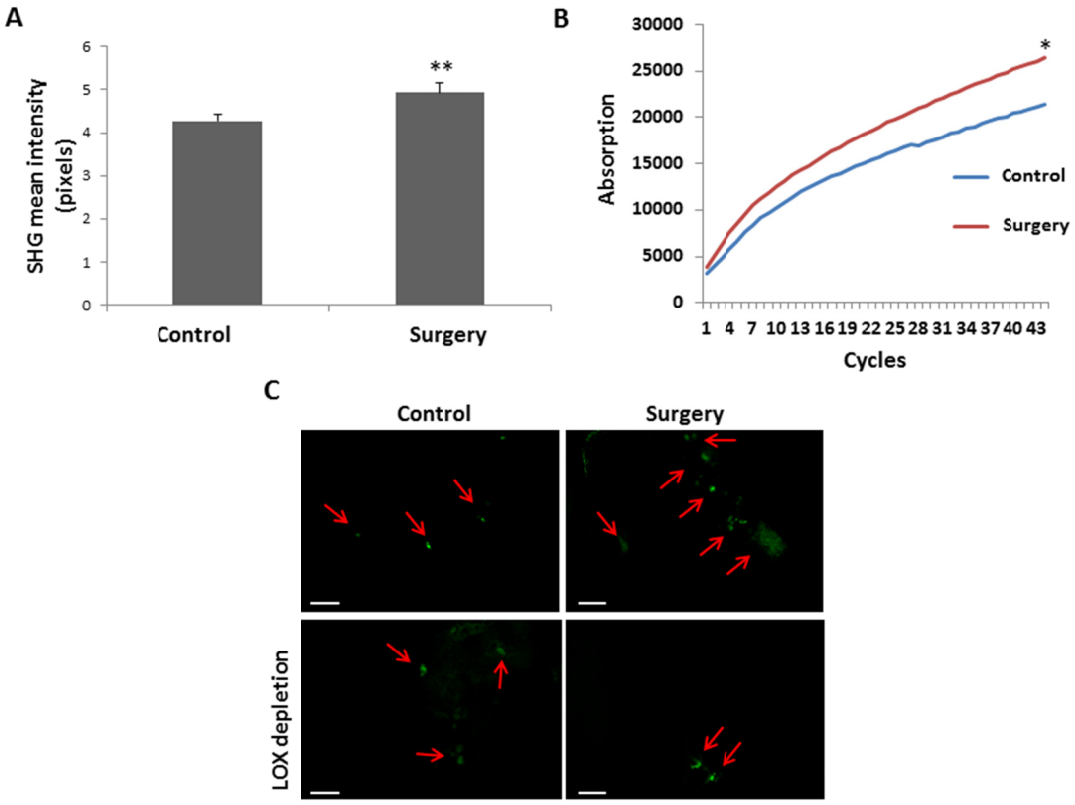

Figure S6 (related to Figure 6): Increased fibrillary collagen, LOX activity, and tumor cell seeding in the lungs of mice injected with post-surgery plasma from patients. (A) Relative collagen intensity in the lungs of mice was measured by two-photon second harmonic generation (SHG) analysis from images presented in Fig. 6G. The fluorescent signal was determined using densitometric analysis (ImageJ). **$p<0.01$ as assessed by two-tailed Student's t-test. (B) Lungs from 8-10 week old CB.17 SCID mice injected with plasma from colorectal cancer patients at baseline or 24 hours after they underwent surgery (n=3 patients; plasma specimen for each mouse) were lysed. The lysates were assessed for LOX activity. LOX activity was assessed by paired Student's t-test. A representative graph from three biological replicates is provided. *$p<0.05$ as assessed by two-tailed Student t-test. (C) Plasma (pooled) from colorectal cancer patients (n=6) at baseline or 24 hours post-surgery was depleted for LOX as described in Experimental Procedures. Subsequently, the plasma was injected into naïve SCID CB.17 mice (n=3 mice/group) and 24 hours later EMT/6-GFP+ cells ($2.5x10^4$) were intravenously injected for PuMA. Lungs were sliced and subsequently cultured in medium for 6 days. Images of lung sections were obtained on day 6 in culture using Leica CTR 6000 system. Red arrows indicate GFP+ cells. Scale bar=200μm.

REFERENCES

Adini, A., Fainaru, O., Udagawa, T., Connor, K.M., Folkman, J., and D'Amato, R.J. (2009). Matrigel cytometry: a novel method for quantifying angiogenesis in vivo. J ImmunolMethods *342*, 78-81.

Erler, J.T., Bennewith, K.L., Nicolau, M., Dornhofer, N., Kong, C., Le, Q.T., Chi, J.T., Jeffrey, S.S., and Giaccia, A.J. (2006). Lysyl oxidase is essential for hypoxia-induced metastasis. Nature *440*, 1222-1226.

Gingis-Velitski, S., Loven, D., Benayoun, L., Munster, M., Bril, R., Voloshin, T., Alishekevitz, D., Bertolini, F., and Shaked, Y. (2011). Host response to short-term, single-agent chemotherapy induces matrix metalloproteinase-9 expression and accelerates metastasis in mice. Cancer Res *71*, 6986-6996.

Hiratsuka, S., Goel, S., Kamoun, W.S., Maru, Y., Fukumura, D., Duda, D.G., and Jain, R.K. (2011). Endothelial focal adhesion kinase mediates cancer cell homing to discrete regions of the lungs via E-selectin up-regulation. Proc Natl Acad Sci U S A *108*, 3725-3730.

Mendoza, A., Hong, S.H., Osborne, T., Khan, M.A., Campbell, K., Briggs, J., Eleswarapu, A., Buquo, L., Ren, L., Hewitt, S.M*., et al.* (2010). Modeling metastasis biology and therapy in real time in the mouse lung. J Clin Invest *120*, 2979-2988.

Philpott, N.J., Turner, A.J., Scopes, J., Westby, M., Marsh, J.C., Gordon-Smith, E.C., Dalgleish, A.G., and Gibson, F.M. (1996). The use of 7-amino actinomycin D in identifying apoptosis: simplicity of use and broad spectrum of application compared with other techniques. Blood *87*, 2244-2251.

Shaked, Y., Ciarrocchi, A., Franco, M., Lee, C.R., Man, S., Cheung, A.M., Hicklin, D.J., Chaplin, D., Foster, F.S., Benezra, R*., et al.* (2006). Therapy-induced acute recruitment of circulating endothelial progenitor cells to tumors. Science *313*, 1785-1787.